

Nuclear Matter and its Role in Supernovae, Neutron Stars and Compact Object Binary Mergers¹

James M. Lattimer^a and Madappa Prakash^a

^a*Dept. of Physics & Astronomy, State University of New York at Stony Brook,
Stony Brook, NY 11794-3800*

Abstract

The equation of state (EOS) of dense matter plays an important role in the supernova phenomenon, the structure of neutron stars, and in the mergers of compact objects (neutron stars and black holes). During the collapse phase of a supernova, the EOS at subnuclear densities controls the collapse rate, the amount of deleptonization and thus the size of the collapsing core and the bounce density. Properties of nuclear matter that are especially crucial are the symmetry energy and the nuclear specific heat. The nuclear incompressibility, and the supernuclear EOS, play supporting roles. In a similar way, although the maximum masses of neutron stars are entirely dependent upon the supernuclear EOS, other important structural aspects are more sensitive to the equation of state at nuclear densities. The radii, moments of inertia, and the relative binding energies of neutron stars are, in particular, sensitive to the behavior of the nuclear symmetry energy. The dependence of the radius of a neutron star on its mass is shown to critically influence the outcome of the compact merger of two neutron stars or a neutron star with a small mass black hole. This latter topic is especially relevant to this volume, since it stems from research prompted by the tutoring of David Schramm a quarter century ago.

Key words: Nuclear Matter; Supernovae; Neutron Stars; Binary Mergers

PACS: 26.50.+x, 26.60.+c, 97.60.Bw, 97.60.Jd, 97.80.-d

¹ Partially supported by USDOE Grants DE-AC02-87ER40317 and DE-FG02-88ER-40388, and by NASA ATP Grant # NAG 52863.

1 Introduction

The equation of state (EOS) of dense matter plays an important role in the supernova phenomenon and in the structure and evolution of neutron stars. Matter in the collapsing core of a massive star at the end of its life is compressed from white dwarf-like densities of about 10^6 g cm^{-3} to two or three times the nuclear saturation density, about $3 \cdot 10^{14} \text{ g cm}^{-3}$ or $n_s = 0.16$ baryons fm^{-3} . The central densities of neutron stars may range up to $5\text{--}10 n_s$. At densities around n_s and below matter may be regarded as a mixture of neutrons, protons, electrons and positrons, neutrinos and antineutrinos, and photons. At higher densities, additional constituents, such as hyperons, kaons, pions and quarks may be present, and there is no general consensus regarding the properties of such ultradense matter. Fortunately for astrophysics, however, the supernova phenomenon and many aspects of neutron star structure may not depend upon ultradense matter, and this article will focus on the properties of matter at lower densities.

The main problem is to establish the state of the nucleons, which may be either bound in nuclei or be essentially free in continuum states. Neither temperatures nor densities are large enough to excite degrees of freedom, such as hyperons, mesons or quarks. Electrons are rather weakly interacting and may be treated as an ideal Fermi gas: at densities above 10^7 g cm^{-3} , they are relativistic. Because of their even weaker interactions, photons and neutrinos (when they are confined in matter) may also be treated as ideal gases.

At low enough densities and temperatures, and provided the matter does not have too large a neutron excess, the relevant nuclei are stable in the laboratory, and experimental information may be used directly. The so-called Saha equation may be used to determine their relative abundances. Under more extreme conditions, there are a number of important physical effects which must be taken into account. At higher densities, or at moderate temperatures, the neutron chemical potential increases to the extent that the density of nucleons outside nuclei can become large. It is then important to treat matter outside nuclei in a consistent fashion with that inside. These nucleons will modify the nuclear surface, decreasing the surface tension. At finite temperatures, nuclear excited states become populated, and these states can be included by treating nuclei as warm drops of nuclear matter. At low temperatures, nucleons in nuclei are degenerate and Fermi-liquid theory is probably adequate for their description. However, near the critical temperature above which the dense phase of matter inside nuclei can no longer coexist with the lighter phase of matter outside nuclei, the equilibrium of the two phases of matter is crucial.

The fact that at subnuclear densities the spacing between nuclei may be of the same order of magnitude as the nuclear size itself will lead to substan-

tial reductions in the nuclear Coulomb energy. Although finite temperature “plasma” effects will modify this, the zero-temperature Wigner-Seitz approximation employed by Baym, Bethe & Pethick (1) is usually adequate. Near the nuclear saturation density, nuclear deformations must be dealt with, including the possibilities of “pasta-like” phases and matter turning “inside-out” (*i.e.*, the dense nuclear matter envelopes a lighter, more neutron-rich, liquid). Finally, the translational energy of the nuclei may be important under some conditions. This energy is important in that it may substantially reduce the average size of the nuclear clusters.

An acceptable way of bridging the regions of low density and temperature, in which the nuclei can be described in terms of a simple mass formula, and high densities and/or high temperatures in which the matter is a uniform bulk fluid, is to use a compressible liquid droplet model for nuclei in which the drop maintains thermal, mechanical, and chemical equilibrium with its surroundings. This allows us to address both the phase equilibrium of nuclear matter, which ultimately determines the densities and temperatures in which nuclei are permitted, and the effects of an external nucleon fluid on the properties of nuclei. Such a model was originally developed by Lattimer *et al.* (2) and modified by Lattimer & Swesty (3). This work was a direct result of David Schramm’s legendary ability to mesh research activities of various groups, in this case to pursue the problem of neutron star decompression. After the fact, the importance of this topic for supernovae became apparent.

2 Nucleon Matter Properties

The compressible liquid droplet model rests upon the important fact that in a many-body system the nucleon-nucleon interaction exhibits saturation. Empirically, the energy per particle of bulk nuclear matter reaches a minimum, about -16 MeV, at a density $n_s \cong 0.16 \text{ fm}^{-3}$. Thus, close to n_s , its density dependence is approximately parabolic. The nucleon-nucleon interaction is optimized for equal numbers of neutrons and protons (symmetric matter), so a parabolic dependence on the neutron excess or proton fraction, x , can be assumed. About a third to a half of the energy change made by going to asymmetric matter is due to the nucleon kinetic energies, and to a good approximation, this varies as $(1 - 2x)^2$ all the way to pure neutron matter ($x = 0$). The x dependence of the potential terms in most theoretical models can also be well approximated by a quadratic dependence. Finally, since at low temperatures the nucleons remain degenerate, their temperature dependence to leading order is also quadratic. Therefore, for analytical purposes, the nucleon free energy per baryon can be approximated as $f_{bulk}(n, x)$, in MeV, as

$$f_{bulk}(n, x) \simeq -16 + S_v(n)(1 - 2x)^2 + \frac{K_s}{18} \left(\frac{n}{n_s} - 1 \right)^2 - \frac{K'_s}{27} \left(\frac{n}{n_s} - 1 \right)^3 - a_v(n, x)T^2, \quad (1)$$

where $a_v(n) = (2m^*/\hbar^2)(\pi/12n)^{2/3}$. The expansion parameters, whose values are uncertain to varying degrees, are the incompressibility, $K_s = 190 - 250$ MeV, the skewness parameter $K'_s = 1780 - 2380$ MeV, the symmetry energy coefficient $S_v \equiv S_v(n_s) = 25 - 36$ MeV, and the bulk level density parameter, $a_v(n_s, x = 1/2) \simeq (1/15)(m^*(n_s, x = 1/2)/m)$ MeV⁻¹, where m^* is the effective mass of the nucleon. Values for $m^*(n_s, x = 1/2)/m$ are in the range 0.7 – 0.9. The general definition of the incompressibility is $K = 9dP/dn = 9d(n^2df_{bulk}/dn)/dn$, where P is the pressure, and $K_s \equiv K(n_s, 1/2)$. It is worthwhile noting that the symmetry energy and nucleon effective mass (which directly affects the matter's specific heat) are density dependent, but these dependencies are difficult to determine from experiments. The parameters, and their density dependences, characterize the nuclear force model and are essential to our understanding of astrophysical phenomena.

The experimental determination of these parameters has come from comparison of the total masses and energies of giant resonances of laboratory nuclei with theoretical predictions. Some of these comparisons are easily illustrated with the compressible liquid droplet model. In this model, the nucleus is treated as uniform drop of nuclear matter with temperature T , density n_i and proton fraction x_i . The nucleus will, in general, be surrounded by and be in equilibrium with a vapor of matter with density n_o and proton fraction x_o . At low ambient densities n and vanishing temperature, the outside vapor vanishes. Even at zero temperature, if n is large enough, greater than the so-called neutron drip density $n_d \simeq 1.6 \cdot 10^{-3}$ fm⁻³, the neutron chemical potential of the nucleus is positive and “free” neutrons exist outside the nucleus. At finite temperature, the external vapor consists of both neutrons and protons. In addition, because of their high binding energy, α -particles will also be present. The total free energy density is the sum of the various components:

$$F = F_H + F_o + F_\alpha + F_e + F_\gamma. \quad (2)$$

Here, F_H and F_o represent the free energy densities of the heavy nuclei and the outside vapor, respectively. The energy densities of the electrons and photons, F_e and F_γ , are independent of the baryons and play no role in the equilibrium. For simplicity, we neglect the role of α -particles in the following discussion (although it is straightforward to include their effect (2)).

In the compressible liquid drop model, it is assumed that the nuclear energy

can be written as an expansion in $A^{1/3}$ and $(1 - 2x_i)^2$:

$$F_H = un_i[f_{bulk} + f_{surf} + f_{Coul} + f_{trans}], \quad (3)$$

where the f 's represent free energies per baryon due to the bulk, surface, Coulomb, and translation, respectively. The bulk energy, for example, is given by Eq. (1). The surface energy can be parametrized as

$$f_{surf} = 4\pi R^2 \sigma(x_i, T) \equiv 4\pi R^2 h(T)[\sigma_o - \sigma_s(1 - 2x_i)^2], \quad (4)$$

where R is the nuclear charge radius, $h(T)$ is a calculable function of temperature, σ_o is the surface tension of symmetric matter, and $\sigma_s = (n_i^2/36\pi)^{1/3} S_s$ where S_s is the surface symmetry energy coefficient from the traditional mass formula. In this simplified discussion, the influence of the neutron skin (2), which distinguishes the ‘‘drop model’’ from the ‘‘droplet model’’, is omitted. The Coulomb energy, in the Wigner-Seitz approximation (1), is

$$f_{Coul} = 0.6x_i^2 A^2 e^2 D(u)/R, \quad (5)$$

where $D(u) = 1 - 1.5u^{1/3} + 0.5u$ and u is the fraction of the volume occupied by nuclei. If the fractional mass of matter outside the nuclei is small, $u \simeq n/n_i$.

It is clear that additional parameters, S_s and another involving the temperature dependence of h , exist in conjunction with those defining the expansions of the bulk energy. The temperature dependence is related to the matter’s critical temperature T_c at which the surface disappears. It is straightforward to demonstrate from the thermodynamic relations defining T_c , namely $\partial P_{bulk}/\partial n = 0$ and $\partial^2 P_{bulk}/\partial n^2 = 0$, that $T_c \propto \sqrt{K_s}$. Therefore, the specific heat to be associated with the surface energy will in general be proportional to $T_c^{-2} \propto K_s^{-1}$. About half the total specific heat originates in the surface, so K_s influences the temperature for a given matter entropy, important during stellar collapse.

The equilibrium between nuclei and their surroundings is determined by minimizing F with respect to its internal variables, at fixed n , Y_e , and T . This is described in more detail in Refs. (2; 3), and leads to equilibrium conditions involving the pressure and the baryon chemical potentials, as well as a condition determining the nuclear size R . The latter is analogous to the one found by Baym, Bethe & Pethick (1) who equated the nuclear surface energy with twice the Coulomb energy. The relations in Eqs. (4) and (5) lead to

$$R = \left[\frac{15\sigma(x_i)}{8\pi e^2 x_i^2 n_i^2} \right]^{1/3}. \quad (6)$$

Experimental limits to K_s , most importantly from RPA analyses of the breathing mode of the giant monopole resonance (4), give $K_s \cong 230$ MeV. It is also possible to obtain values from the so-called scaling model developed from the compressible liquid drop model. The finite-nucleus incompressibility is

$$K(A, Z) = (M/\hbar^2)R^2 E_{br}^2, \quad (7)$$

where M is the mass of the nucleus and E_{br} is the breathing-mode energy. $K(A, Z)$ is commonly expanded as

$$K(A, Z) = K_s + K_{surf}A^{-1/3} + K_{vI}I^2 + K_{surfI}I^2A^{-1/3} + K_C Z^2 A^{-4/3}, \quad (8)$$

and then fit by least squares to the data for E_{br} . Here the asymmetry $I = 1 - 2Z/A$. For a given assumed value of K_s , and taking $K_{surfI} = 0$, Pearson (5) showed that experimental data gave

$$K_C \simeq 15.4 - 0.065K_s \pm 2 \text{ MeV}, \quad K_{surf} \simeq 230 - 3.2K_s \pm 50 \text{ MeV}. \quad (9)$$

With minimal assumptions regarding the form of the nuclear force, Pearson (5) demonstrated that values of K_s ranging from 200 MeV to more than 350 MeV could be consistent with experimental data.

But the liquid drop model predicts other relations between the parameters:

$$\begin{aligned} K(A, Z) &= R^2 \left. \frac{\partial^2 E(Z, A)/A}{\partial R^2} \right|_A = 9n^2 \left. \frac{\partial^2 E(Z, A)/A}{\partial n^2} \right|_A, \\ 0 = P(A, Z) &= R \left. \frac{\partial E(Z, A)/A}{\partial R} \right|_A = 3n \left. \frac{\partial E(Z, A)/A}{\partial n} \right|_A. \end{aligned} \quad (10)$$

Here $E(Z, A)$ is the total energy of the nucleus, and is equivalent to Eq. (3). The second of these equations simply expresses the equilibrium between the nucleus and the surrounding vacuum, which implies that the pressure of the bulk matter inside the nucleus is balanced by the pressure due to the curvature of the surface and the Coulomb energy. It can then be shown that

$$\begin{aligned} K_C &= -(3e^2/5r_o)[8 + 27n_s^3 f'''_{bulk}(n_s)/K_s], \\ K_{surf} &= 4\pi r_o^2 \sigma_o [9n_s^2 \sigma_o''/\sigma_o + 22 + 54n_s^3 f'''_{bulk}(n_s)/K_s], \\ K_{surfI} &= 4\pi r_o^2 \sigma_s [9n_s^2 \sigma_s''/\sigma_s + 22 + 54n_s^3 f'''_{bulk}(n_s)/K_s], \\ K_I &= 9[n_s^2 S''_v(n_s) - 2n_o S'_v(n_s) - 9n_s^4 S'_v(n_s) f'''_{bulk}(n_s)/K_s]. \end{aligned} \quad (11)$$

Primes denote derivatives with respect to the density. From these relations,

and again assuming $K_{surfI} = 0$, Pearson demonstrated that an interesting correlation between K_s and K'_s , where $K'_s \equiv -27n_s^3 f'''_{bulk}(n_s)$, could be obtained:

$$K'_s = -0.0860K_s^2 + (28.37 \pm 2.65)K_s. \quad (12)$$

Assuming $K_s \simeq 190 - 250$ MeV, this suggests that $K'_s = 1780 - 2380$ MeV, a potential constraint. Alternatively, eliminating K'_s , one finds

$$K_s = 137.4 - 26.36n_s^2\sigma''/\sigma_o \pm 23.2 \text{ MeV}. \quad (13)$$

The second derivative of the surface tension can be deduced from Hartree-Fock or Thomas-Fermi semi-infinite surface calculations. For example, if a parabolic form of f_{bulk} is used, one finds

$$n_s^2\sigma''/\sigma_o = -6 \quad (14)$$

leading to $K_s = 295.5 \pm 23.2$ MeV. In general, the density dependence of S_v will decrease the magnitudes of K_s and σ'' from the above values.

It is hoped current experimental work will tighten these constraints. A shortcoming of the scaling model is that, to date, the surface symmetry energy term was neglected. This is not required, however, and further work is necessary to resolve this matter.

Because the surface energy represents the energy difference between uniformly and realistically distributed nuclear material in a nucleus, the parameter S_s can be related to the density dependence of $S_v(n)$ and to K_s . If f_{bulk} is assumed to behave quadratically with density around n_s , this relation can be particularly simply expressed (6):

$$\frac{S_s}{S_v} = \frac{3}{\sqrt{2}} \frac{a_{1/2}}{r_o} \int_0^1 \frac{\sqrt{x}}{1-x} \left[\frac{S_v}{S_v(xn_s)} - 1 \right] dx. \quad (15)$$

Here, $S_v \equiv S_v(n_s)$, $a_{1/2} = (dr/d \ln n)_{n_s/2}$ is a measure of the thickness of the nuclear surface and $r_o = (4\pi n_s/3)^{-1/3} = R/A^{1/3}$. If $S_v(n)$ is linear, then the integral is 2; if $S_v(n) \propto n^{2/3}$, then the integral is 0.927. Since $a_{1/2}$ will be sensitive to the value of K_s , we expect the value of S_s/S_v to be also.

Experimentally, there are two major sources of information regarding the symmetry energy parameters: nuclear masses and giant resonance energies. However, because of the small excursions in $A^{1/3}$ afforded by laboratory nuclei, each source provides only a correlation between S_s and S_v . For example, the

total symmetry energy in the liquid droplet model (now explicitly including the presence of the neutron skin, see Ref. (2)) is

$$E_{sym} = (1 - 2x_i)^2 S_v / [1 + (S_s/S_v)A^{-1/3}]. \quad (16)$$

Evaluating $\alpha = d \ln S_s / d \ln S_v$ near the “best-fit” values S_{s0} and S_{v0} , one finds

$$\alpha \simeq 2 + S_{v0} < A >^{1/3} / S_{s0} \simeq 6, \quad (17)$$

where $< A >^{1/3}$ for the fitted nuclei is about 5. Thus, as the value of S_v is changed in the mass formula, the value of S_s must vary rapidly to compensate.

An additional correlation between these parameters can be obtained from the fitting of isovector giant resonances, and this has the potential of breaking the degeneracy of S_v and S_s , because it has a different slope (6). Lipparini & Stringari (7) used a hydrodynamical model of the nucleus to derive the isovector resonance energy:

$$\begin{aligned} E_d &= \sqrt{\frac{24\hbar^2}{m^*} \frac{NZ}{A} \left[\int \frac{nr^2 S_v}{S_v(n)} d^3r \right]^{-1}} \\ &\simeq 96.5 \sqrt{\frac{m}{m^*} \frac{S_v}{30 \text{ MeV}} \left[1 + \frac{5S_s}{3S_v A^{1/3}} \right]^{-1}} A^{-1/3} \text{ MeV}, \end{aligned} \quad (18)$$

where m^* is an effective nucleon mass. This relation results in a slightly less-steep correlation between S_s and S_v ,

$$\alpha = 2/m^* + (3/5)S_{v0} < A >^{1/3} / S_{s0} \simeq 4 - 5. \quad (19)$$

Unfortunately the value of m^* is an undetermined parameter and this slope is not very different from that obtained from fitting masses. Therefore, uncertainties in the model make a large difference to the crossing point of these two correlations. A strong theoretical attack, perhaps using further RPA analysis, together with more experiments to supplement the relatively meager amount of existing data, would be very useful.

3 The Equation of State and the Collapse of Massive Stars

Massive stars at the end of their lives are believed to consist of a white dwarf-like iron core of 1.2–1.6 M_\odot having low entropy ($s \leq 1$), surrounded by layers

of less processed material from shell nuclear burning. The effective Chandrasekhar mass, the maximum mass the degenerate electron gas can support, is dictated by the entropy and the average lepton content, Y_L , believed to be around 0.41–0.43. As mass is added to the core by shell Si-burning, the core eventually becomes unstable and collapses.

During the collapse, the lepton content decreases due to net electron capture on nuclei and free protons. But when the core density approaches 10^{12} g cm $^{-3}$, the neutrinos can no longer escape from the core on the dynamical collapse time (8). After neutrinos become trapped, Y_L is frozen at a value of about 0.38–0.40, and the entropy is also thereafter fixed. The core continues to collapse until the rapidly increasing pressure reverses the collapse at a bounce density of a few times nuclear density.

The immediate outcome of the shock generated by the bounce is also dependent upon Y_L . First, the shock energy is determined by the net binding energy of the post-bounce core, and is proportional to $Y_e^{10/3}$ (9). Second, the shock is largely dissipated by the energy required to dissociate massive nuclei in the still-infalling matter of the original iron core outside the post-bounce core. The larger the Y_L of the core, the larger its mass and the smaller this shell. Therefore, the progress of the shock is very sensitive to the value of Y_L .

The final value of Y_L is controlled by weak interaction rates, and is strongly dependent upon the fraction of free protons, X_p , which is proportional to $\exp(\mu_p/T)$, and the phase space available for proton capture on nuclei, which is proportional to $\mu_e - \hat{\mu}$, where $\hat{\mu} = \mu_n - \mu_p$. Both are sensitive to the proton fraction in nuclei (x_i) and are largely controlled by Y_L . In addition, the specific heat controls the temperature which has a direct influence upon the free proton abundance and the net electron capture rate. In spite of the intricate feedback, nuclear parameters relating chemical potentials to composition, especially S_v and S_s , are obviously important.

As an example, consider $\hat{\mu} = \mu_n - \mu_p = -n_i^{-1} \partial F_H / \partial x_i$. With the model of Eqs. (3)-(5), one has

$$\hat{\mu} = 4S_v(1 - 2x_i) - \left(\frac{72\pi e^2 D}{5x_i n_i} \right)^{1/3} \frac{\sigma_o - \sigma_s(1 - 2x_i)(1 - 6x_i)}{(\sigma_o - \sigma_s(1 - 2x_i)^2)^{1/3}}. \quad (20)$$

Recall that $\sigma_s \propto S_s$. Although the bulk and Coulomb terms alone (Eq. 20 with $\sigma_s = 0$) imply that $\hat{\mu}$ for a given x_i rises with increasing S_v , the proper inclusion of the surface symmetry energy gives rise to the opposite behavior. This is illustrated in Fig. 1.

Uncertainties in nuclear parameters can thus be expected to have an influence upon the collapse of massive stars, for example, in the collapse rate, the final

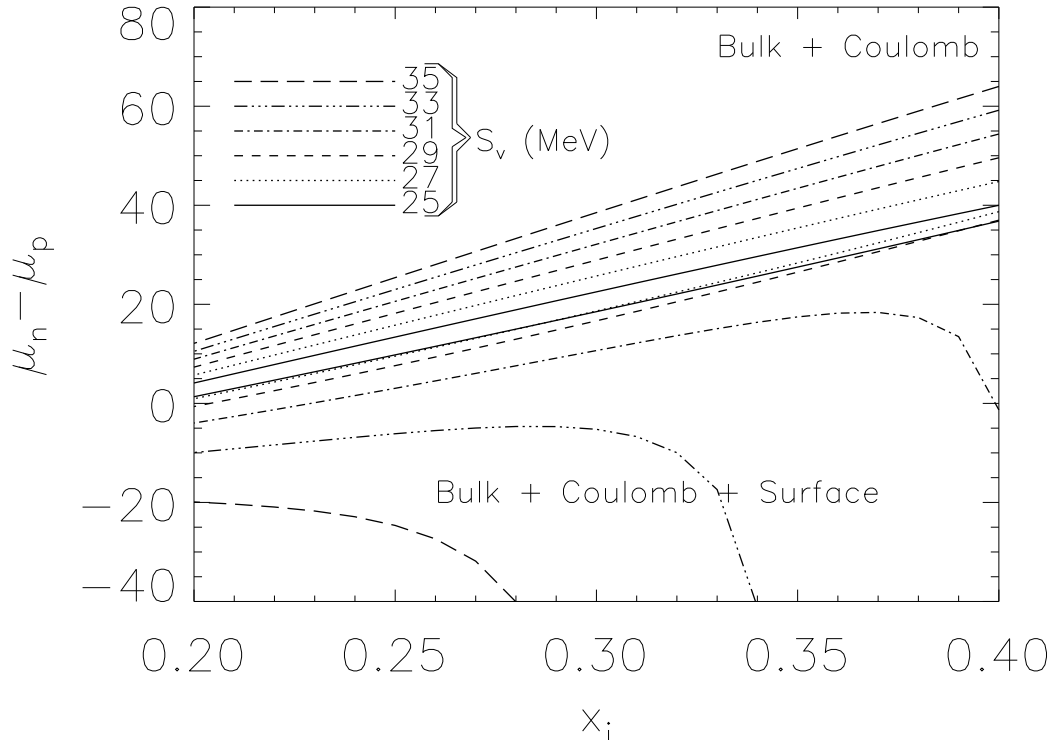


Fig. 1. Comparison of $\hat{\mu} = \mu_n - \mu_p$ as a function of x_i for various assumed values of S_v , both including and excluding the effects of the surface symmetry energy.

trapped lepton fraction, and the radius at which the bounce-generated shock initially stalls. Swesty, Lattimer & Myra (10) investigated the effects upon stellar collapse of altering parameters in a fashion constrained by nuclear systematics. They found that as long as the parameters permitted a neutron star maximum mass above the PSR1913+16 mass limit ($1.44 M_\odot$), the shock generated by core bounce consistently stalls near 100 km, independently of the assumed K_s in the range 180–375 MeV and S_v in the range 27–35 MeV. Ref. (10) also found that the final trapped lepton fraction is also apparently independent of variations in both K_s and S_v . These results are in contrast to earlier simulations which had used EOSs that could not support cold, catalyzed $1.4 M_\odot$ stars, or in which S_s was not varied consistently with S_v . The strong feedback between the EOS, weak interactions, neutrino transport, and hydrodynamics is an example of *Mazurek's Law*.

In fact, the only significant consequence of varying S_v involved the pre-bounce neutrino luminosities. Increasing S_v increases the electron capture rate (proportional to $\mu_e - \hat{\mu}$ and therefore increases the ν_e luminosity during collapse, as shown in Fig. 2. Nevertheless, the collapse rate also increases, so that neutrino trapping occurs sooner and the final trapped lepton fraction does not change. It is possible that large neutrino detectors such as Super-Kamiokande or SNO may be able to observe an enhanced early rise in neutrino luminosity from nearby galactic supernovae.

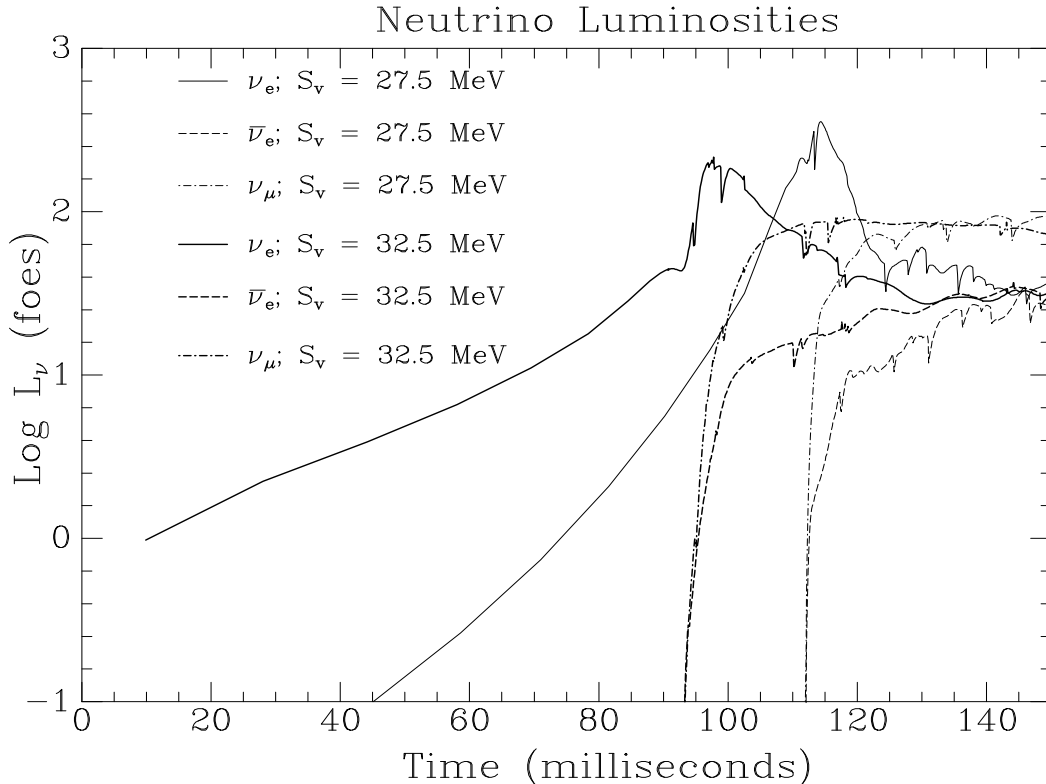


Fig. 2. The neutrino luminosities during infall as a function of the bulk symmetry energy parameter.

4 The Structure of Neutron Stars

The theoretical study of the structure of neutron stars is crucial if new observations of masses and radii are to lead to effective constraints on the EOS of dense matter. This study becomes ever more important as laboratory studies may be on the verge of yielding evidence about the composition and stiffness of matter beyond n_s . To date, several accurate mass determinations of neutron stars are available, and they all lie in a narrow range ($1.25 - 1.44 M_\odot$). There is some speculation that the absence of neutron stars with masses above $1.5 M_\odot$ implies that M_{max} for neutron stars has approximately this value. However, since fewer than 10 neutron stars have been weighed, and all these are in binaries, this conjecture is premature. Theoretical studies of dense matter indicate that considerable uncertainties exist in the high-density behavior of the EOS largely because of the poorly constrained many-body interactions. These uncertainties are reflected in a significant uncertainty in the maximum mass of a beta-stable neutron star, which ranges from $1.5-2.5 M_\odot$.

There is some theoretical support for a lower mass limit for neutron stars in the range $1.1 - 1.2 M_\odot$. This follows from the facts that the collapsing core of a massive star is always greater than $1 M_\odot$ and the minimum mass of a

protoneutron star with a low-entropy inner core of $\sim 0.6 M_{\odot}$ and a high-entropy envelope is at least $1.1 M_{\odot}$. Observations from the Earth of thermal radiation from neutron star surfaces could yield values of the quantity $R_{\infty} = R/\sqrt{1 - 2GM/Rc^2}$, which results from redshifting the stars luminosity and temperature. $M - R$ trajectories for representative EOSs (discussed below) are shown in Figure 3. It appears difficult to simultaneously have $M > 1M_{\odot}$ and $R_{\infty} < 12$ km. Those pulsars with at least some suspected thermal radiation generically yield effective values of R_{∞} so small that it is believed that the radiation originates from polar hot spots rather than from the surface as a whole. Other attempts to deduce a radius include analyses (14) of X-ray bursts from sources 4U 1705-44 and 4U 1820-30 which implied rather small values, $9.5 < R_{\infty} < 14$ km. However, the modeling of the photospheric expansion and touchdown on the neutron star surface requires a model dependent relationship between the color and effective temperatures, rendering these estimates uncertain. Absorption lines in X-ray spectra have also been investigated with a view to deducing the neutron star radius. Candidates for the matter producing the absorption lines are either the accreted matter from the companion star or the products of nuclear burning in the bursts. In the former case, the most plausible element is thought to be Fe, in which case the relation $R \approx 3.2GM/c^2$, only slightly larger than the minimum possible value based upon causality, (15; 16) is inferred. In the latter case, plausible candidates are Ti and Cr, and larger values of the radius would be obtained. In both cases, serious difficulties remain in interpreting the large line widths, of order 100–500 eV, in the 4.1 ± 0.1 keV line observed from many sources. A first attempt at using light curves and pulse fractions from pulsars to explore the $M - R$ relation suggested relatively large radii, of order 15 km (17). However, this method, which assumed dipolar magnetic fields, was unable to satisfactorily reconcile the calculated magnitudes of the pulse fractions and the shapes of the light curves with observations.

Prospects for a radius determination have improved in recent years, however, with the detection of a nearby neutron star, RX J185635-3754, in X-rays and optical radiation (18). The observed X-rays, from the ROSAT satellite, are consistent with blackbody emission with an effective temperature of about 57 eV and very little extinction. In addition, the fortuitous location of the star in the foreground of the R CrA molecular cloud limits the distance to $D < 120$ pc. The fact that the source is not observable in radio and its lack of variability in X-rays implies that it is not a pulsar unlike other identified radio-silent isolated neutron stars. This gives the hope that the observed radiation is not contaminated with non-thermal emission as is the case for pulsars. The X-ray observations of RXJ185635-3754 alone yield $R_{\infty} \approx 7.3(D/120 \text{ pc})$ km for a best-fit blackbody. Such a value is too small to be consistent with any neutron star with more than $1 M_{\odot}$. But the optical flux is about a factor of 2.5 brighter than what is predicted for the X-ray blackbody, which is consistent

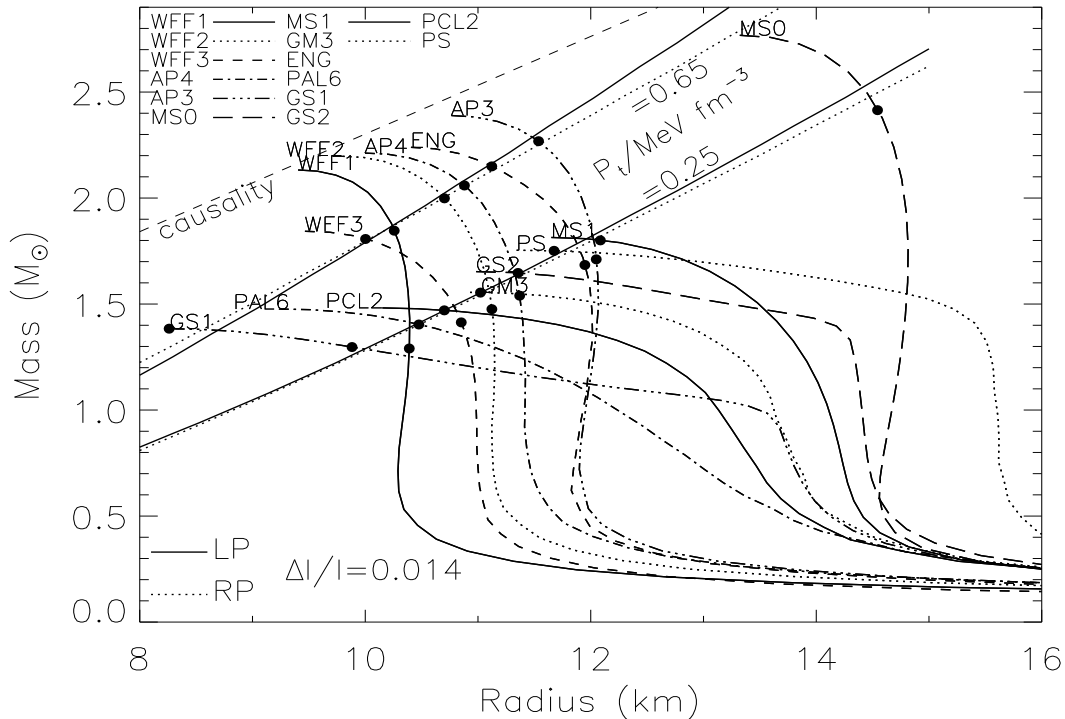


Fig. 3. $M - R$ curves for the EOSs listed in Table 1. The diagonal lines represent two theoretical estimates (LP=Ref. (11); RP=Ref. (12)) of the locus of points for $\Delta I/I = 1.4\%$ for extremal limits of P_t , 0.25 and 0.65 MeV fm^{-3} . The large dots on the $M - R$ curves are the exact results. The region to the left of the contours labeled 0.65 is not allowed if current glitch models are correct (13).

with there being a heavy-element atmosphere (19). With such an atmosphere, it is found (20) that the effective temperature is reduced to approximately 50 eV and R_∞ is also increased, to a value of approximately $21.6(D/120 \text{ pc}) \text{ km}$. Upcoming parallax measurements with the Hubble Space Telescope should permit a distance determination to about 10-15% accuracy. If X-ray spectral features are discovered with the planned Chandra and XMM space observatories, the composition of the neutron star atmosphere can be inferred, and the observed redshifts will yield independent mass and radius information. In this case, *both* the mass and radius of this star will be found.

Furthermore, a proper motion of $0.34'' \text{ yr}^{-1}$ has been detected, in a direction that is carrying the star away from the Upper Scorpius (USco) association (20). With an assumed distance of about 80 pc, the positions of RX J185635-3754 and this association overlap about 800,000 years ago. The runaway OB star ζ Oph is also moving away from USco, appearing to have been ejected on the order of a million years ago. The superposition of these three objects is interesting, and one can speculate that this is not coincidental. If upcoming parallax measurements are consistent with a distance to RX J185635-3754 of about 80 pc, the evidence for this scenario will be strong, and a good age estimate will result.

Table 1

Equations of state used in this work. Approach refers to the basic theoretical paradigm. Composition refers to strongly interacting components (n=neutron, p=proton, H=hyperon, K=kaon, Q=quark); all approaches include leptonic contributions.

Symbol	Reference	Approach	Composition
FP	(21)	Variational	np
PS	(22)	Potential	$n\pi^0$
WFF(1-3)	(23)	Variational	np
AP(1-4)	(24)	Variational	np
MS(1-3)	(25)	Field Theoretical	np
MPA(1-2)	(26)	Dirac-Brueckner HF	np
ENG	(27)	Dirac-Brueckner HF	np
PAL(1-6)	(28)	Schematic Potential	np
GM(1-3)	(29)	Field Theoretical	npH
GS(1-2)	(30)	Field Theoretical	npK
PCL(1-2)	(31)	Field Theoretical	npHQ
SQM(1-3)	(31)	Quark Matter	Q (u, d, s)

In this section, a striking empirical relationship is noted which connects the radii of neutron stars and the pressure of matter in the vicinity of n_s . In addition, a number of analytic, exact, solutions to the general relativistic TOV equation of hydrostatic equilibrium are explored that lead to several useful approximations for neutron star structure which directly correlate observables such as masses, radii, binding energies, and moments of inertia. The binding energy, of which more than 99% is carried off in neutrinos, will be revealed from future neutrino observations of supernovae. Moments of inertia are connected with glitches observed in the spin down of pulsars, and their observations yield some interesting conclusions about the distribution of the moment of inertia within the rotating neutron star. From such comparisons, it may become easier to draw conclusions about the dense matter EOS when firm observations of neutron star radii or moments of inertia become available to accompany the several known accurate mass determinations.

4.1 Neutron Star Radii

The composition of a neutron star chiefly depends on the nature of strong interactions, which are not well understood in dense matter. The several pos-

sible models investigated (15; 32) can be conveniently grouped into three broad categories: nonrelativistic potential models, field-theoretical models, and relativistic Dirac-Brueckner-Hartree-Fock models. In each of these approaches, the presence of additional softening components such as hyperons, Bose condensates or quark matter, can be incorporated.

Figure 3 displays the mass-radius relation for several recent EOSs (the abbreviations are explained in Table 1). Even a cursory glance indicates that in the mass range from $1 - 1.5 M_{\odot}$ it is usually the case that the radius has little dependence upon the mass. The lone exception is the model GS1, in which a kaon condensate, leading to considerable softening, appears. While it is generally assumed that a stiff EOS leads to both a large maximum mass and a large radius, many counter examples exist. For example, MS3 has a relatively small maximum mass but has large radii compared to most other EOSs with larger maximum masses. Also, not all EOSs with extreme softening have small radii (viz., GS2). Nonetheless, for stars with mass greater than $1 M_{\odot}$, only models with a large degree of softening can have $R_{\infty} < 12$ km. Should the radius of a neutron star ever be accurately determined to satisfy $R_{\infty} < 12$ km, a strong case can be made for the existence of extreme softening.

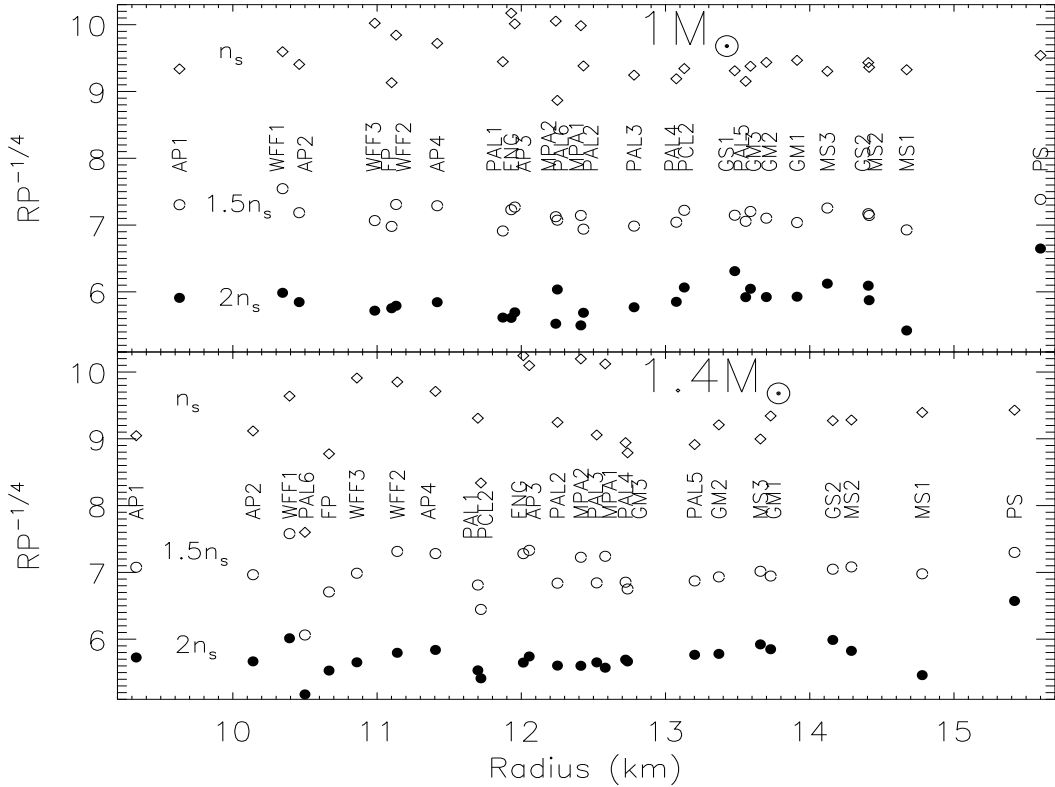


Fig. 4. Empirical relation between P and R for various EOSs (see Table 1 for details). The upper and lower panels show results for gravitational masses of $1 M_{\odot}$ and $1.4 M_{\odot}$, respectively. Symbols show $PR^{-1/4}$ in units of $\text{MeV fm}^{-3} \text{ km}^{-1/4}$ at the three indicated fiducial densities.

It is relevant that a Newtonian polytrope with $n = 1$ has the property that the stellar radius is independent of both the mass and central density. In fact, numerical relativists have often approximated equations of state with $n = 1$ polytropes. An $n = 1$ polytrope has the property that the radius is proportional to the square root of the constant K in the polytropic pressure law $P = K\rho^{1+1/n}$. This suggests that there might be a quantitative relation between the radius and the pressure that does not depend upon the equation of state at the highest densities, which determines the overall softness or stiffness (and hence, the maximum mass).

To make the relation between matter properties and the nominal neutron star radius definite, Fig. 4 shows the remarkable empirical correlation which exists between the radii of 1 and 1.4 M_\odot stars and the matter’s pressure evaluated at densities of 1, 1.5 and 2 n_s . Table 1 explains the EOS symbols used in Fig. 4. Despite the relative insensitivity of radius to mass for a particular “normal” equation of state, the nominal radius R_M , which is defined as the radius at a particular mass M in solar units, still varies widely with the EOS employed. Up to ~ 5 km differences are seen in $R_{1.4}$, for example, in Fig. 4. This plot is restricted to EOSs which have maximum masses larger than about 1.55 M_\odot and to those which do not have strong phase transitions (such as those due to a Bose condensate or quark matter). Such EOSs violate these correlations, especially for the case of 1.4 M_\odot stars. We emphasize that this correlation is valid only for cold, catalyzed neutron stars, i.e., it will not be valid for protonneutron stars which have finite entropies and might contain trapped neutrinos. The correlation has the form

$$R \simeq \text{constant} \cdot [P(n)]^{0.23-0.26}, \quad (21)$$

where P is the total pressure inclusive of leptonic contributions evaluated at the density n . An exponent of 1/4 was chosen for display in Fig. 4, but the correlation holds for a small range of exponents about this value. The correlation is marginally tighter for the baryon density $n = 1.5n_s$ and $2n_s$ cases. Thus, instead of the power 1/2 that the Newtonian polytrope relations would predict, a power of approximately 1/4 is suggested when the effects of relativity are included. The value of the constant in Eq. (21) depends upon the chosen density, and can be obtained from Fig. 4.

The exponent of 1/4 can be quantitatively understood by using a relativistic generalization of the $n = 1$ polytrope, due to Buchdahl (33). For the EOS

$$\rho = 12\sqrt{p_*P} - 5P, \quad (22)$$

where p_* is a constant, there is an analytic solution to Einstein’s equations:

$$\begin{aligned}
e^\nu \equiv g_{tt} &= (1 - 2\beta)(1 - \beta - u)(1 - \beta + u)^{-1}; \\
e^\lambda \equiv g_{rr} &= (1 - 2\beta)(1 - \beta + u)(1 - \beta - u)^{-1}(1 - \beta + \beta \cos Ar')^{-2}; \\
8\pi PG/c^4 &= A^2 u^2 (1 - 2\beta)(1 - \beta + u)^{-2}; \\
8\pi \rho G/c^2 &= 2A^2 u (1 - 2\beta)(1 - \beta - 3u/2)(1 - \beta + u)^{-2}; \\
u &= \beta (Ar')^{-1} \sin Ar'; \quad r = r'(1 - \beta + u)(1 - 2\beta)^{-1}; \\
A^2 &= 288\pi p_* G c^{-4} (1 - 2\beta)^{-1}; \quad R = \pi(1 - \beta)(1 - 2\beta)^{-1} A^{-1}. \quad (23)
\end{aligned}$$

The free parameters of this solution are $\beta \equiv GM/Rc^2$ and the scale p_* . Note that $R \propto p_*^{-1/2}(1 + \beta^2/2 + \dots)$, so for a given value of p_* , the radius increases only very slowly with mass, exactly as expected from an $n = 1$ Newtonian polytrope. It is instructive to analyze the response of R to a change of pressure at some fiducial density ρ , for a fixed mass M . One finds

$$\left. \frac{d \ln R}{d \ln P} \right|_{\rho, M} = \frac{\left. \frac{d \ln R}{d \ln p_*} \right|_{\beta} \left. \frac{d \ln p_*}{d \ln P} \right|_{\rho}}{1 + \left. \frac{d \ln R}{d \ln \beta} \right|_{p_*}} = \left(1 - \frac{5}{6} \sqrt{\frac{P}{p_*}} \right) \frac{(1 - \beta)(1 - 2\beta)}{2(1 - 3\beta + 3\beta^2)}. \quad (24)$$

In the limit $\beta \rightarrow 0$, $P \rightarrow 0$ and $d \ln R/d \ln P \rightarrow 1/2$, the value characteristic of an $n = 1$ Newtonian polytrope. Finite values of β and P render the exponent smaller than $1/2$. If the stellar radius is about 15 km, $p_* = \pi/(288R^2) \approx 4.85 \cdot 10^{-5} \text{ km}^{-2}$. If the fiducial density is $\rho \approx 1.5m_b n_s \approx 2.02 \cdot 10^{-4} \text{ km}^{-2}$ (with m_b the baryon mass), Eq. (22) implies that $P \approx 8.5 \cdot 10^{-6} \text{ km}^{-2}$. For $M = 1.4 M_\odot$, the value of β is 0.14, and $d \ln R/d \ln P \simeq 0.31$. This result is mildly sensitive to the choices for ρ and R , and the Buchdahl solution is not a perfect representation of realistic EOSs; nevertheless, it provides a reasonable explanation of the correlation in Eq. (21).

The existence of this correlation is significant because, in large part, the pressure of degenerate matter near the nuclear saturation density n_s is determined by the symmetry properties of the EOS. Thus, the measurement of a neutron star radius, if not so small as to indicate extreme softening, could provide an important clue to the symmetry properties of matter. In either case, valuable information is obtained.

The specific energy of nuclear matter near the saturation density may be expressed as an expansion in the asymmetry $(1 - 2x)$, as displayed in Eq. (1), that can be terminated after the quadratic term (28). Leptonic contributions must be added to Eq. (1) to obtain the total energy and pressure; the electron energy per baryon is $f_e = (3/4)\hbar c x(3\pi^2 n x)^{1/3}$. Matter in neutron stars is in beta equilibrium, i.e., $\mu_e - \mu_n + \mu_p = \partial(f_{\text{bulk}} + f_e)/\partial x = 0$, so the electronic contributions may be eliminated to recast the pressure as (34)

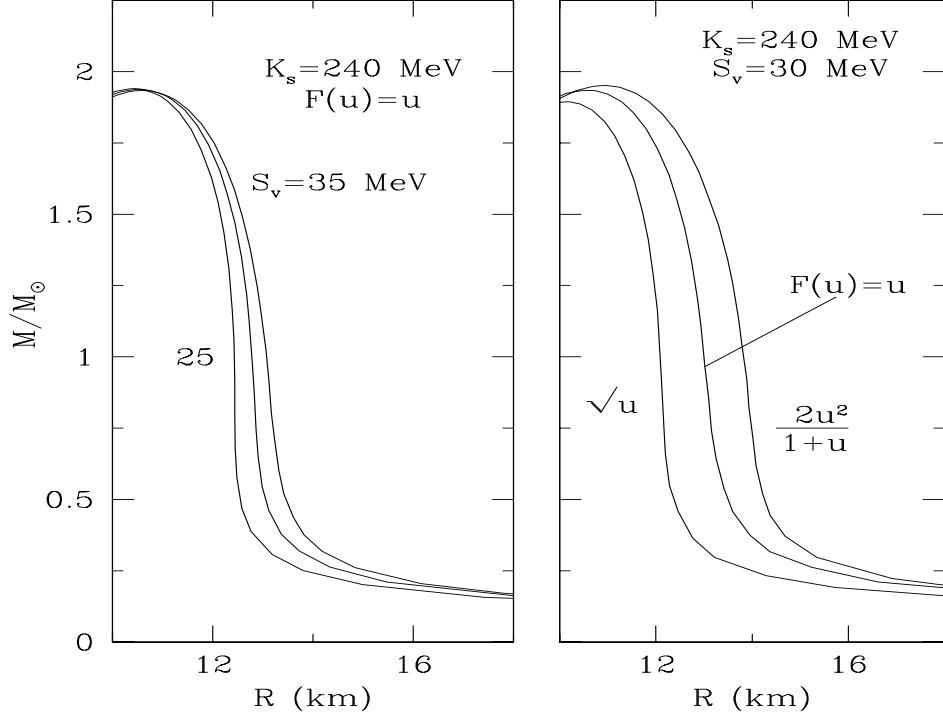


Fig. 5. Left panel: $M - R$ curves for selected PAL parametrizations (28) showing the sensitivity to symmetry energy. The left panel shows variations arising from different choices of the symmetry energy at the nuclear saturation density $S_v = S_v(n_s)$; the right panel shows variations arising from different choices of the density dependence of the potential part of the symmetry energy $F(u) = S_v(n)/S_v(n_s)$ where $u = n/n_s$.

$$P = n^2 \left[S'_v(n)(1 - 2x)^2 + \frac{xS_v(n)}{n}(1 - 2x) + \frac{K_s}{9n_s} \left(\frac{n}{n_s} - 1 \right) - \frac{K'_s}{54n_s} \left(\frac{n}{n_s} - 1 \right)^2 \right], \quad (25)$$

where x is now the beta equilibrium value. At the saturation density,

$$P_s = n_s(1 - 2x_s)[n_s S'_v(n_s)(1 - 2x_s) + S_v x_s], \quad (26)$$

where the equilibrium proton fraction at n_s is

$$x_s \simeq (3\pi^2 n_s)^{-1} (4S_v/\hbar c)^3 \simeq 0.04 \quad (27)$$

for $S_v = 30$ MeV. Due to the small value of x_s , one finds that $P_s \simeq n_s^2 S'_v(n_s)$. If the pressure is evaluated at a larger density, other nuclear parameters besides S_v and $S'_v(n_s)$, become significant. For $n = 2n_s$, one thus has

$$P(2n_s) \simeq 4n_s [n_s S'_v(2n_s) + (K_s - K'_s/6)/9]. \quad (28)$$

If it is assumed that $S_v(n)$ is linear in density, $K_s \sim 220$ MeV and $K'_s \sim 2000$ MeV (as indicated in Eq. 12), the symmetry contribution is still about 70% of the total.

The sensitivity of the radius to the symmetry energy is graphically shown by the parametrized EOS of PAL (28) in Fig. 5. The symmetry energy function $S_v(n)$ is a direct input in this parametrization. The figure shows the dependence of mass-radius trajectories as the quantities S_v and $S_v(n)$ are alternately varied. Clearly, the density dependence of $S_v(n)$ is more important in determining the neutron star radius. Note also the weak sensitivity of the maximum neutron star mass to S_v .

At present, experimental guidance concerning the density dependence of the symmetry energy is limited and mostly based upon the division of the nuclear symmetry energy between volume and surface contributions, as discussed in the previous section. Upcoming experiments involving heavy-ion collisions (at GSI, Darmstadt), which might sample densities up to $\sim (3 - 4)n_s$, will be limited to analyzing properties of the symmetric nuclear matter EOS through a study of matter, momentum, and energy flow of nucleons. Thus, studies of heavy nuclei far off the neutron drip lines will be necessary in order to pin down the properties of the neutron-rich regimes encountered in neutron stars.

4.2 Neutron Star Moments of Inertia and Binding Energies

Besides the stellar radius, other global attributes of neutron stars are potentially observable, including the moment of inertia and the binding energy. These quantities depend primarily upon the ratio M/R as opposed to details of the EOS, as can be readily seen by evaluating them using analytic solutions to Einstein's equations. Although over 100 analytic solutions to Einstein's equations are known (35), nearly all of them are physically unrealistic. However, three analytic solutions are of particular interest in neutron star structure.

The first is the well-known Schwarzschild interior solution for an incompressible fluid, $\rho = \rho_c$, where ρ is the mass-energy density. This is mostly of interest because it determines the maximum compression $\beta = GM/Rc^2$ for a neutron star, namely 4/9, based upon the pressure being finite. Two aspects of the incompressible fluid that are physically unrealistic, however, include the fact that the sound speed is everywhere infinite, and that the density does not vanish on the star's surface.

The second analytic solution, B1, due to Buchdahl (33), is described in Eq. (23).

The third analytic solution (TolVII) was discovered by Tolman (36) in 1939,

and is the case when the mass-energy density ρ varies quadratically, that is,

$$\rho = \rho_c[1 - (r/R)^2]. \quad (29)$$

In fact, this is an adequate representation, as displayed in Fig. 6 for neutron stars more massive than $1.2 M_\odot$. The equations of state used are listed in Table 1. The largest deviations from this general relation exist for models with extreme softening (GS1, GS2, PCL2) and which have relatively low maximum masses (see Fig. 3). It is significant that all models must, of course, approach this behavior at both extremes $r \rightarrow 0$ and $r \rightarrow R$.

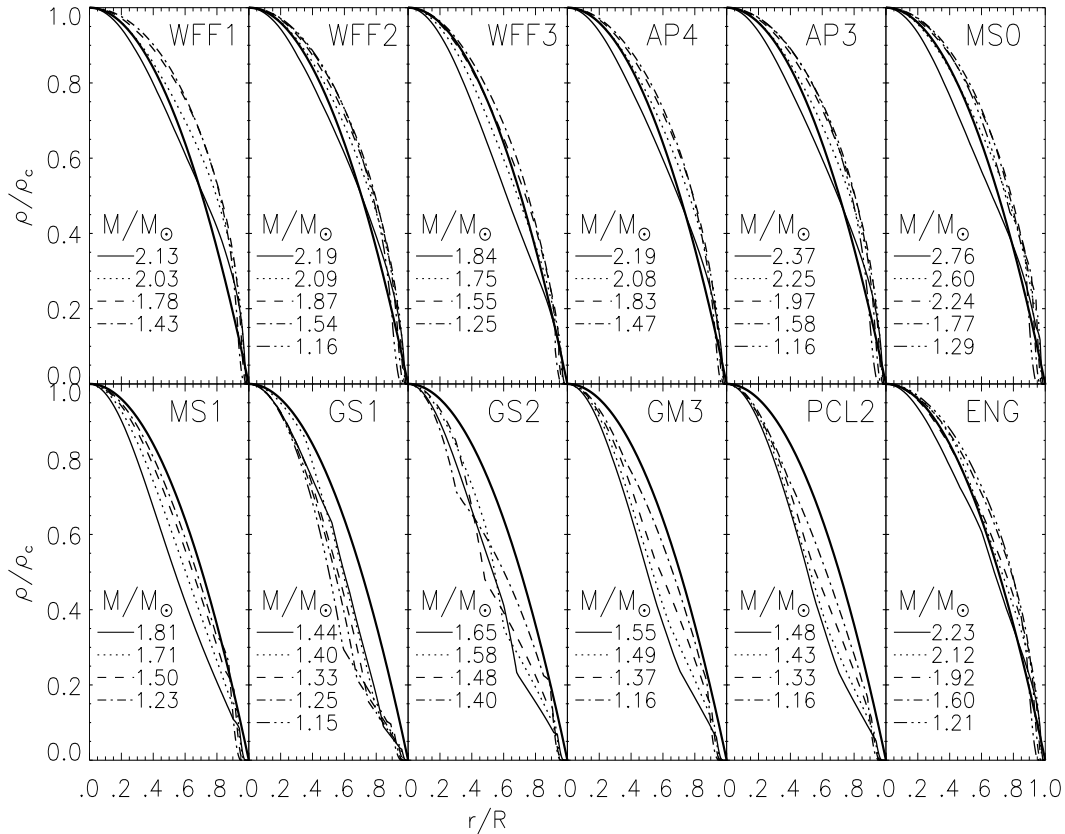


Fig. 6. Each panel shows mass-energy density profiles in the interiors of selected stars (masses indicated) ranging from about $1.2 M_\odot$ to the maximum mass (solid line) for the given equation of state (see Table 1). The thick black lines show the simple quadratic approximation $1 - (r/R)^2$.

Because the Tolman solution is often overlooked in the literature (for exceptions, see, for example, Refs. (35; 37)) it is summarized here. It is useful in establishing interesting and simple relations that are insensitive to the equation of state. In terms of the variable $x = r^2/R^2$ and the parameter β , the assumption $\rho = \rho_c(1 - x)$ results in $\rho_c = 15\beta c^2/(8\pi G R^2)$. The solution of Einstein's equations for this density distribution is:

$$\begin{aligned}
e^{-\lambda} &= 1 - \beta x(5 - 3x), & e^\nu &= (1 - 5\beta/3) \cos^2 \phi, \\
P &= \frac{c^4}{4\pi R^2 G} [\sqrt{3\beta e^{-\lambda}} \tan \phi - \frac{\beta}{2}(5 - 3x)], & n &= \frac{\rho c^2 + P \cos \phi}{m_b c^2 \cos \zeta}, \\
\phi &= (w_1 - w)/2 + \zeta, & \phi_c &= \phi(x = 0), & \zeta &= \tan^{-1} \sqrt{\beta/[3(1 - 2\beta)]}, \\
w &= \log[x - 5/6 + \sqrt{e^{-\lambda}/(3\beta)}], & w_1 &= w(x = 1).
\end{aligned} \tag{30}$$

The central values of $P/\rho c^2$ and c_s^2 are

$$\left. \frac{P}{\rho c^2} \right|_c = \frac{2}{15} \sqrt{\frac{3}{\beta}} \left(\frac{c_{sc}}{c} \right)^2, \quad \left(\frac{c_{sc}}{c} \right)^2 = \tan \phi_c \left(\tan \phi_c + \sqrt{\frac{\beta}{3}} \right). \tag{31}$$

This solution, like that of Buchdahl's, is scale-free, with the parameters β and ρ_c (or M or R). Here, n is the baryon density, m_b is the nucleon mass, and c_{sc} is the sound speed at the star's center. When $\phi_0 = \pi/2$, or $\beta \approx 0.3862$, P_c becomes infinite, and when $\beta \approx 0.2698$, c_{sc} becomes causal (i.e., c). Recall that for an incompressible fluid, P_c becomes infinite when $\beta = 4/9$. For the Buchdahl solution, P_c becomes infinite when $\beta = 2/5$ and the causal limit is reached when $\beta = 1/6$. For comparison, if causality is enforced at high densities, it has been empirically determined that $\beta < 0.34$ (15; 16).

The general applicability of these exact solutions can be gauged by analyzing the moment of inertia, which, for a star uniformly rotating with angular velocity Ω , is

$$I = (8\pi/3) \int_0^R r^4 (\rho + P/c^2) e^{(\lambda-\nu)/2} (\omega/\Omega) dr. \tag{32}$$

The metric function ω is a solution of the equation

$$d[r^4 e^{-(\lambda+\nu)/2} \omega']/dr + 4r^3 \omega de^{-(\lambda+\nu)/2}/dr = 0 \tag{33}$$

with the surface boundary condition

$$\omega_R = \Omega - \frac{R}{3} \omega'_R = \Omega \left[1 - \frac{2GI}{R^3 c^2} \right]. \tag{34}$$

The second equality in the above follows from the definition of I and the TOV equation. Writing $j = \exp[-(\nu + \lambda)/2]$, the TOV equation becomes

$$j' = -4\pi Gr(P/c^2 + \rho) j e^\lambda / c^2. \tag{35}$$

Then, one has

$$I = -\frac{2c^2}{3G} \int \frac{\omega}{\Omega} r^3 dj = \frac{c^2 R^4 \omega'_R}{6G\Omega}. \quad (36)$$

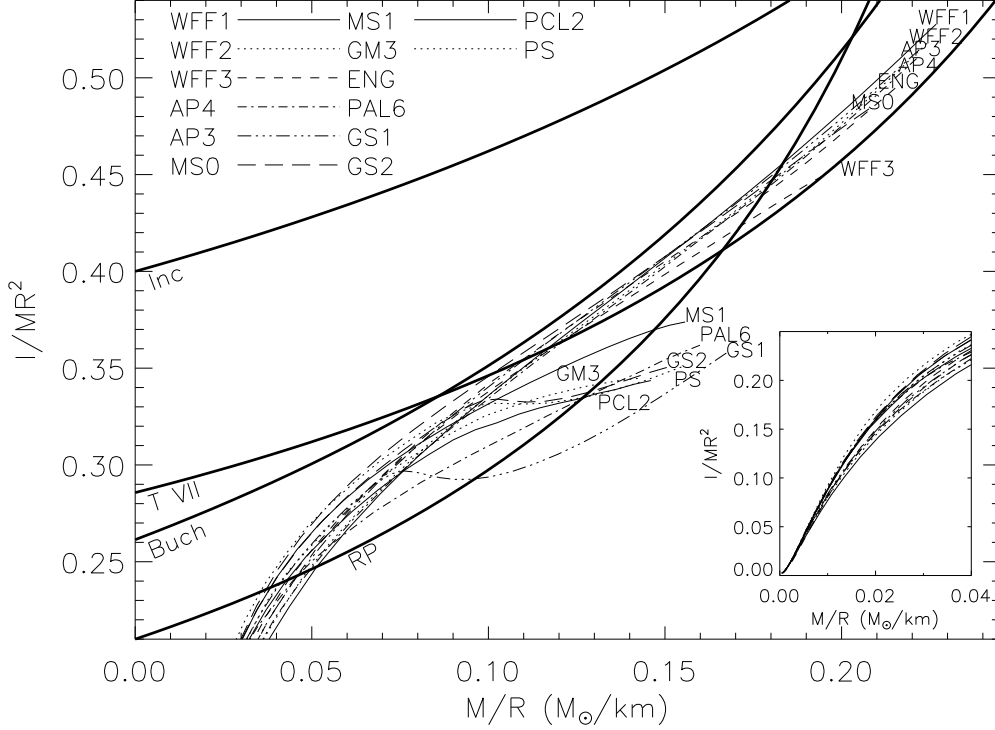


Fig. 7. The moment of inertia I in units of MR^2 for the equations of state listed in Table 1. I_{Inc} , I_{B1} , I_{VII} and I_{RP} are approximations described in the text.

Unfortunately, an analytic representation of ω or the moment of inertia for any of the three exact solutions is not available. However, approximations which are valid to within 0.5% are

$$I_{Inc}/MR^2 \simeq 2(1 - 0.87\beta - 0.3\beta^2)^{-1}/5, \quad (37)$$

$$I_{B1}/MR^2 \simeq (2/3 - 4/\pi^2)(1 - 1.81\beta + 0.47\beta^2)^{-1}, \quad (38)$$

$$I_{TVII}/MR^2 \simeq 2(1 - 1.1\beta - 0.6\beta^2)^{-1}/7. \quad (39)$$

In each case, the small β limit reduces to the corresponding Newtonian results. Fig. 7 indicates that the Tolman approximation is rather good. Ravenhall & Pethick (12) suggested that the expression

$$I_{RP}/MR^2 \simeq 0.21/(1 - 2u) \quad (40)$$

was a good approximation for the moment of inertia; however, we find that this expression is not a good overall fit, as shown in Fig. 7. For low-mass stars ($\beta < 0.12$), none of these approximations is suitable, but it is unlikely

that any neutron stars are this rarefied. It should be noted that the Tolman approximation does not adequately approximate some EOSs, especially ones that are relatively soft, such as GM3, GS1, GS2, PAL6 and PCL2.

The binding energy formally represents the energy gained by assembling N baryons. If the baryon mass is m_b , the binding energy is simply $BE = Nm_b - M$ in mass units. However, the quantity m_b has various interpretations in the literature. Some authors assume it is about $940 \text{ MeV}/c^2$, the same as the neutron or proton mass. Others assume it is about $930 \text{ MeV}/c^2$, corresponding to the mass of $\text{C}^{12}/12$ or $\text{Fe}^{56}/56$. The latter would yield the energy released in a supernova explosion, which consists of the energy released by the collapse of a white-dwarf-like iron core, which itself is considerably bound. The difference, 10 MeV per baryon, corresponds to a shift of $10/940 \simeq 0.01$ in the value of BE/M . In any case, the binding energy is directly observable from the detection of neutrinos from a supernova event; indeed, it would be the most precisely determined aspect.

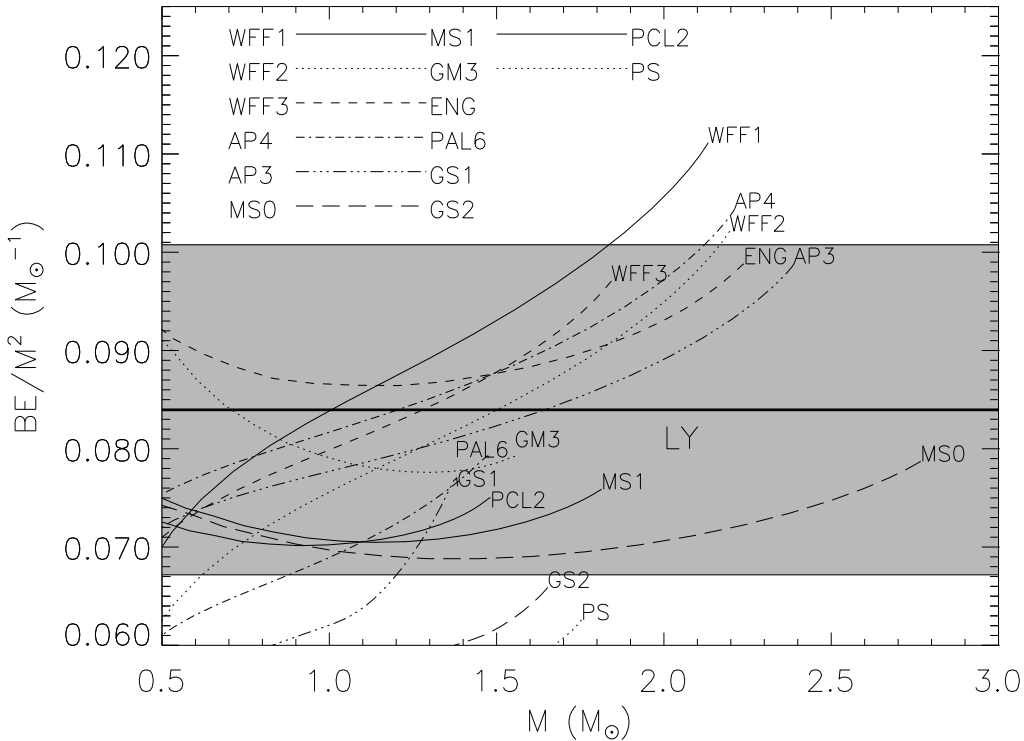


Fig. 8. The binding energy of neutron stars as a function of stellar mass for the equations of state listed in Table 1. The predictions of Eq. (41) are shown by the shaded region.

Lattimer & Yahil (38) suggested that the binding energy could be approximated as

$$BE \approx 1.5 \cdot 10^{51} (M/M_\odot)^2 \text{ ergs} = 0.084 (M/M_\odot)^2 M_\odot. \quad (41)$$

This formula, in general, is accurate to about $\pm 20\%$. The largest deviations are for extremely soft EOSs, as shown in Fig. 8.

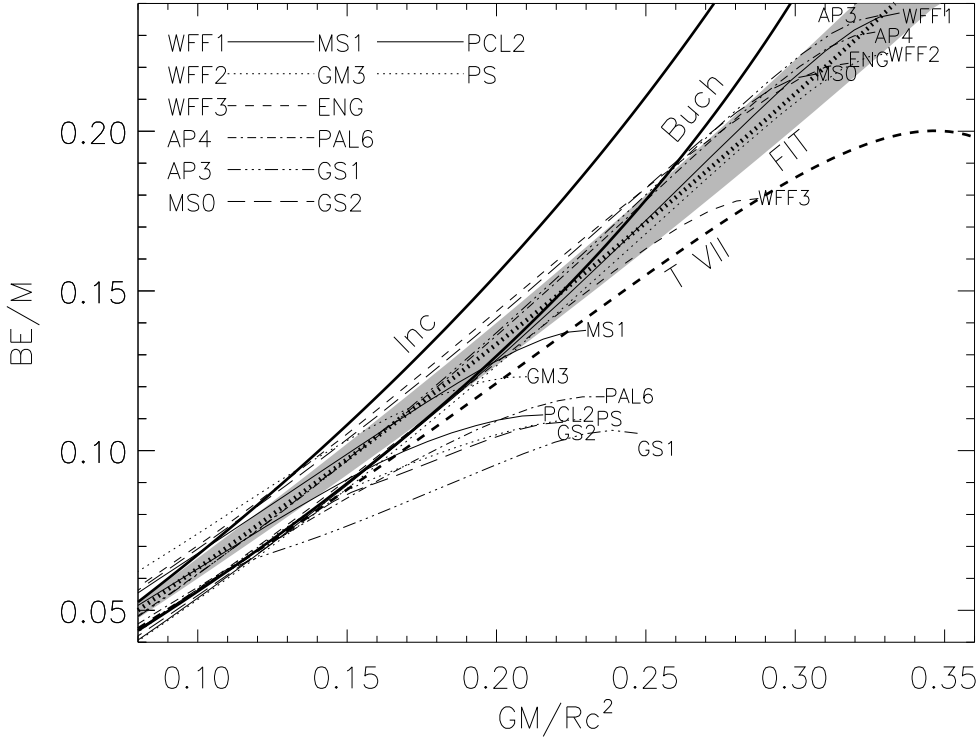


Fig. 9. The binding energy per unit gravitational mass as a function of compactness for the equations of state listed in Table 1. The shaded region shows the prediction of Eq. (42) with $\pm 5\%$ errors.

However, a more accurate representation of the binding energy is given by

$$BE/M \simeq 0.6\beta/(1 - 0.5\beta), \quad (42)$$

which incorporates some radius dependence. Thus, the observation of supernova neutrinos, and the estimate of the total radiated neutrino energy, will yield more accurate information about M/R than about M alone.

In the cases of the incompressible fluid and the Buchdahl solution, analytic results for the binding energy can be found:

$$BE_{Inc}/M = \frac{3}{4\beta} \left(\frac{\sin^{-1} \sqrt{2\beta}}{\sqrt{2\beta}} - \sqrt{1 - 2\beta} \right) - 1, \quad (43)$$

$$BE_{B1}/M = (1 - 1.5\beta)\sqrt{1 - 2\beta}(1 - \beta)^{-1} - 1. \quad (44)$$

The analytic results, the Tolman VII solution, and the fit of Eq. (42) are compared to some recent equations of state in Fig. 9. It can be seen that,

except for very soft cases like PS, PCL2, PAL6, GS1 and GS2, both the Tolman VII and Buchdahl solutions are rather realistic.

4.3 Crustal Fraction of the Moment of Inertia

In the investigation of pulsar glitches, many models associate the glitch size with the fraction of the moment of inertia which resides in the star's crust, usually defined to be the region in which dripped neutrons coexist with nuclei. The high-density crust boundary is set by the phase boundary between nuclei and uniform matter, where the pressure is P_t and the density n_t . The low-density boundary is the neutron drip density, or for all practical purposes, simply the star's surface since the amount of mass between the neutron drip point and the surface is negligible. We define ΔR to be the distance between the points where the density is n_t and zero. One can apply Eq. (32) to determine the moment of inertia of the crust alone with the assumptions that $P/c^2 \ll \rho$, $m(r) \simeq M$, and $\omega j \simeq \omega_R$ in the crust. One finds

$$\Delta I \simeq \frac{8\pi \omega_R}{3 \Omega} \int_{R-\Delta R}^R \rho r^4 e^{\lambda} dr \simeq \frac{8\pi \omega_R}{3GM \Omega} \int_0^{P_t} r^6 dP, \quad (45)$$

where M is the star's total mass and the TOV equation was used in the last step. In the crust, the fact that the EOS is of the approximate polytropic form $P \simeq K\rho^{4/3}$ can be used to find an approximation for the integral $\int r^6 dP$, *viz.*

$$\int_0^{P_t} r^6 dP \simeq P_t R^6 \left[1 + \frac{2P_t}{n_t m_n c^2} \frac{(1+7\beta)(1-2\beta)}{\beta^2} \right]^{-1}. \quad (46)$$

Since the approximation Eq. (42) gives I in terms of M and R , and ω_R/Ω is given in terms of I and R in Eq. (34), the quantity $\Delta I/I$ can thus be expressed as a function of M and R with the only dependence upon the equation of state (EOS) arising from the values of P_t and n_t ; there is no explicit dependence upon the higher-density EOS. However, the major dependence is upon the value of P_t , since n_t enters only as a correction. We then find

$$\frac{\Delta I}{I} \simeq \frac{28\pi P_t R^3}{3Mc^2} \frac{(1-1.67\beta-0.6\beta^2)}{\beta} \left[1 + \frac{2P_t}{n_t m_b c^2} \frac{(1+7\beta)(1-2\beta)}{\beta^2} \right]^{-1}. \quad (47)$$

In general, the EOS parameter P_t , in the units of MeV fm⁻³, varies over the range $0.25 < P_t < 0.65$ for realistic EOSs. The determination of this parameter requires a calculation of the structure of matter containing nuclei

just below nuclear matter density that is consistent with the assumed nuclear matter EOS. Unfortunately, few such calculations have been performed. Like the fiducial pressure at and above nuclear density which appears in the relation Eq. (21), P_t should depend sensitively upon the behavior of the symmetry energy near nuclear density.

Choosing $n_t = 0.07 \text{ fm}^{-3}$, we compare Eq. (47) in Fig. 3 with full structural calculations. The agreement is good. We also note that Ravenhall & Pethick (12) developed a different, but nearly equivalent, formula for the quantity $\Delta I/I$ as a function of M, R, P_t and μ_t , where μ_t is the neutron chemical potential at the core-crust phase boundary. This prediction is also displayed in Fig. 3.

Link, Epstein & Lattimer (13) established a lower limit to the radii of neutron stars by using a constraint derived from pulsar glitches. They showed that glitches represent a self-regulating instability for which the star prepares over a waiting time. The angular momentum requirements of glitches in the Vela pulsar indicate that more than 0.014 of the star's moment of inertia drives these events. If glitches originate in the liquid of the inner crust, this means that $\Delta I/I > 0.014$. A minimum radius can be found by combining this constraint with the largest realistic value of P_t from any equation of state. Stellar models that are compatible with this constraint must fall to the right of the $P_t = 0.65 \text{ MeV fm}^{-3}$ contour in Fig. 3. This imposes a constraint upon the radius, namely that $R > 3.6 + 3.9M/M_\odot \text{ km}$.

5 The Merger of a Neutron Star with a Low-Mass Black Hole

The general problem of the origin and evolution of systems containing a neutron star and a black hole was first detailed by Lattimer & Schramm (39), although the original motivation was due to Schramm. Although speculative at the time, Schramm insisted that this would prove to be an interesting topic from the points of view of nucleosynthesis and gamma-ray emission. The contemporaneous discovery (40) of the first-known binary system containing twin compact objects, PSR 1913+16, which was also found to have an orbit which would decay because of gravitational radiation within 10^{10} yr, bolstered his argument. Eventually, this topic formed the core of Lattimer's thesis (41), and the recent spate of activity, a quarter century later, in the investigation of the evolution and mergers of such compact systems has wonderfully demonstrated Schramm's prescience.

Compact binaries form naturally as the result of evolution of massive stellar binaries. The estimated lower mass limit for supernovae (and neutron star or black hole production) is approximately $8 M_\odot$. Observationally, the number of binaries formed within a given logarithmic separation is approximately

constant, but the relative mass distributions are uncertain. There is some indication that the distribution in binary mass ratios might be flat. The number of possible progenitor systems can then be estimated. Most progenitor systems do not survive the more massive star becoming a supernova. In the absence of a kick velocity it is easily found that the loss of more than half of the mass from the system will unbind it. However, the fact that pulsars are observed to have mean velocities in excess of a few hundred km/s implies that neutron stars are usually produced with large “kick” velocities originating in the supernova explosion. In the case that the kick velocity, which is thought to be randomly directed, opposes the star’s orbital velocity, the chances of the post-supernova binary remaining intact increases. In addition, the separation in a surviving binary will be reduced significantly. Subsequent evolution then progresses to the supernova explosion of the companion. More of these systems survive because in many cases the more massive component explodes. But the surviving systems should both have greatly reduced separations and orbits with high eccentricity.

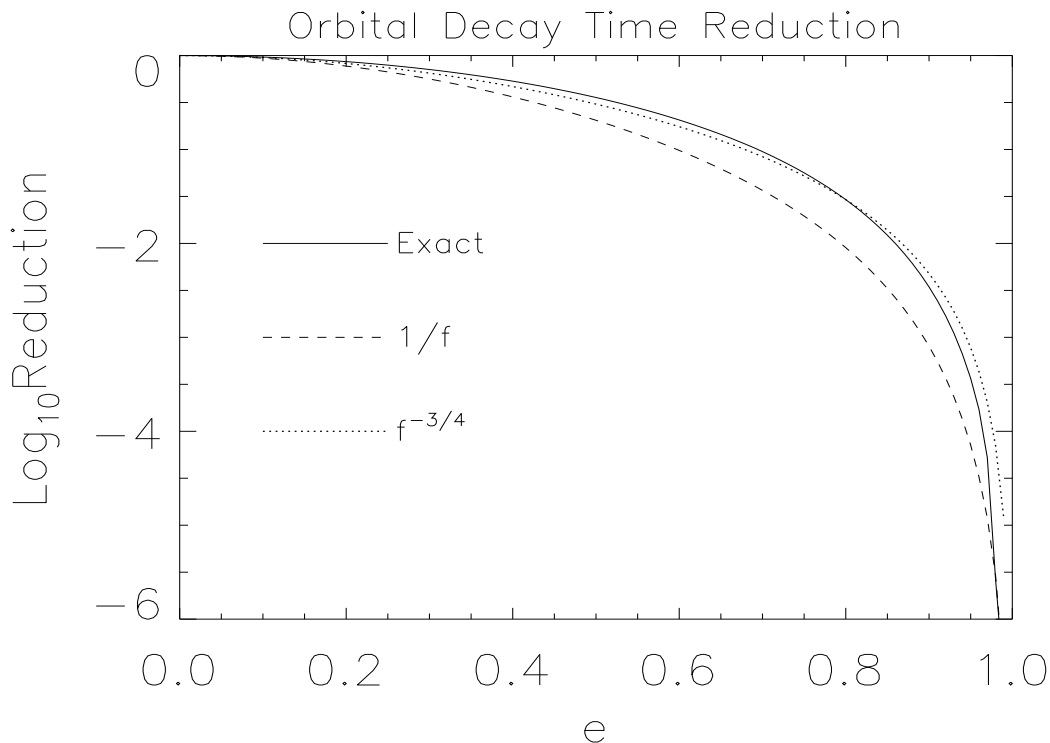


Fig. 10. The reduction of the gravitational radiation orbital decay time as a function of initial orbital eccentricity. The dashed line is the inverse of the Peters (42) f function; the dotted line shows $f^{-3/4}$, which reasonably reproduces the exact result.

Gravitational radiation then causes the binary’s orbit to decay, such that circular orbits of two masses M_1 and M_2 with initial semimajor axes a satisfying

$$a < 2.8[M_1M_2(M_1 + M_2)/M_\odot^3]^{1/4}R_\odot, \quad (48)$$

will fully decay within the age of the Universe ($\sim 10^{10}$ yr). Highly eccentric orbits will decay much faster, as shown in Fig. 10. The dashed curve shows the inverse of the factor (42) by which the gravitational wave luminosity of an eccentric system exceeds that of a circular system:

$$f = (1 + 73e^2/24 + 37e^4/96)(1 - e^2)^{-7/2}. \quad (49)$$

Because the eccentricity also decays, the exact reduction factor is not as strong as $1/f$. A reasonable approximation to the exact result is $f^{-3/4}$, shown by the dotted line in Fig. 10. The coefficient 2.8 in Eq. (48) is increased by a factor of $f^{-3/16}$ or about 2 for moderate eccentricities.

Ref. (39) argued that mergers of neutron stars and black holes, and the subsequent ejection of a few percent of the neutron star's mass, could easily account for all the r -process nuclei in the cosmos. Ref. (39) is also the earliest reference to the idea that compact object binary mergers are associated with gamma-ray bursts. A later seminal contribution by Eichler, Livio, Piran & Schramm (43) argued that mergers of neutron stars occur frequently enough to explain the origin of gamma-ray bursters.

Since the timescale of gamma-ray bursts, being of order seconds to several minutes, is much longer than the coalescence timescale of a binary merger (which is of order the orbital frequency at the last stable orbit, a few milliseconds), it is believed that a coalescence involves the formation of an accretion disc. Although neutrino emission from accreting material, resulting in neutrino-antineutrino annihilation along the rotational axis, has been proposed as a source of gamma rays, it seems more likely that amplification of magnetic fields within the disc might trigger observed bursts. In either case, the lifetime of the accretion disc is still problematic, if it is formed by the breakup of the neutron star near the Roche limit. Its lifetime would probably be only about a hundred times greater than the orbital frequency, or less than a second. However, this timescale would be considerably enhanced if the accretion disc could be formed at larger radii than the Roche limit. A possible mechanism is stable mass transfer from the neutron star to the black hole that would cause the neutron star to spiral away as it loses mass (44; 45).

The classical Roche limit is based upon an incompressible fluid of density ρ and mass M_2 in orbit about a mass M_1 . In Newtonian gravity, this limit is

$$R_{Roche,Newt} = (M_1/0.0901\pi\rho)^{1/3} = 19.2(M_1/M_\odot\rho_{15})^{1/3} \text{ km}, \quad (50)$$

where $\rho_{15} = \rho/10^{15} \text{ g cm}^{-3}$. Using general relativity, Fishbone (46) found that at the last stable circular orbit (including the case when the black hole is rotating) the number 0.0901 in Eq. (50) becomes 0.0664. In geometrized

units, $R_{Roche}/M_1 = 13(14.4)(M_1^2 \rho_{15}/M_\odot^2)^{-1/3}$, where the numerical coefficient refers to the Newtonian (last stable orbit in GR) case. In other words, if the neutron star's mean density is $\rho_{15} = 1$, the Roche limit is encountered beyond the last stable orbit if the black hole mass is less than about $5.9 M_\odot$. Thus, for small enough black holes, mass overflow and transfer from the neutron star to the black hole could begin outside the last stable circular orbit. And, as now discussed, the mass transfer may proceed stably for some considerable time. In fact, the neutron star might move to 2–3 times the orbital radius where mass transfer began. This would provide a natural way to lengthen the lifetime of an accretion disc, by simply increasing its size.

The final evolution of a compact binary is now discussed. Define $q = m_{ns}/M_{BH}$, $\mu = m_{ns}M_{BH}/M$, and $M = M_{BH} + m_{ns}$, where m_{ns} and M_{BH} are the neutron star and black hole masses, respectively. The orbital angular momentum is

$$J^2 = G\mu^2 Ma = GM^3 a q^2 / (1 + q)^4. \quad (51)$$

We can employ Paczyński's (47) formula for the Roche radius of the secondary:

$$R_\ell/a = 0.46[q/(1 + q)]^{1/3}, \quad (52)$$

or a better fit by Eggleton (48):

$$R_\ell/a = 0.49[.6 + q^{-2/3} \ln(1 + q^{1/3})]^{-1}. \quad (53)$$

The orbital separation a at the moment of mass transfer is obtained by setting $R_\ell = R$, the neutron star radius. For stable mass transfer, the star's radius has to increase more quickly than the Roche radius as mass is transferred. Thus, we must have, using Paczyński's formula,

$$\frac{d \ln R}{d \ln m_{ns}} \equiv \alpha \geq \frac{d \ln R_\ell}{d \ln m_{ns}} = \frac{d \ln a}{d \ln m_{ns}} + \frac{1}{3} \quad (54)$$

for stable mass transfer. α is defined in this expression, and is shown in Fig. 11 for a typical EOS. If the mass transfer is conservative, then $\dot{J} = \dot{J}_{GW}$, where

$$\dot{J}_{GW} = -\frac{32}{5} \frac{G^{7/2}}{c^5} \frac{\mu^2 M^{5/2}}{a^{7/2}} = -\frac{32}{5} \frac{G^{7/2}}{c^5} \frac{q^2 M^{9/2}}{(1 + q)^4 a^{7/2}} \quad (55)$$

and

$$\frac{\dot{J}}{J} = \frac{\dot{a}}{2a} + \frac{\dot{q}(1 - q)}{q(1 + q)}. \quad (56)$$

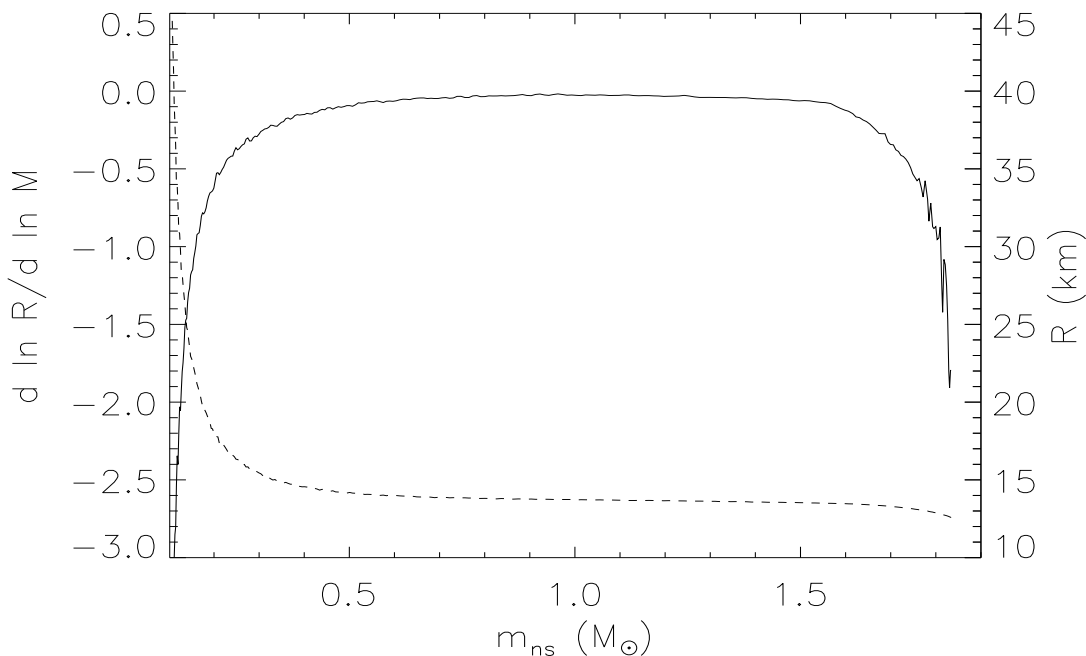


Fig. 11. $d \ln R / d \ln m_{ns} \equiv \alpha$ (solid curve) and neutron star radius R (dashed curve) as functions of neutron star mass m_{ns} for a typical dense matter equation of state.

This leads to

$$\dot{q} \left(\frac{\alpha}{2} + \frac{5}{6} - q \right) \geq -\frac{32 G^3}{5 c^5} \frac{q^2 M^3}{(1+q)a^4}. \quad (57)$$

Since $m_{ns} < M_{BH}$, $\dot{q} \leq 0$, and the condition for stable mass transfer is simply $q \leq 5/6 + \alpha/2$. For moderate mass neutron stars, $\alpha \approx 0$, so in this case the condition is simply $q \leq 5/6$, which might even be achievable in a binary neutron star system. Had we used the more exact formula of Eggleton, Eq. (53), we would have found $q \leq 0.78$. Note that it has often been assumed that $R \propto m_{ns}^{-1/3}$ in such discussions (45), which is equivalent to $\alpha = -1/3$. This is unjustified, and results in the upper limit $q = 2/3$ which might inappropriately rule out stable mass transfer in the case of two neutron stars.

A number of other conditions must hold for stable mass transfer to occur. First, the orbital separation a at the onset must exceed the last stable orbit around the black hole, so that $a > 6GM_{BH}/c^2$, or

$$q \geq 6 \frac{R_\ell}{a} \frac{GM_{BH}}{Rc^2}. \quad (58)$$

Second, the tidal bulge raised on the neutron star must stay outside of the black hole's Schwarzschild radius. Kochanek (44) gives an estimate of the

height of the tidal bulge needed to achieve the required mass loss rate:

$$\frac{\Delta r}{R} = \left[\frac{-\dot{q}}{\beta_t(1+q)\Omega} \right]^{1/3}, \quad (59)$$

where β_t is a dimensionless parameter of order 1 and $\Omega = G^{1/2}M^{1/2}/a^{3/2}$ is the orbital frequency. For \dot{q} we use the equality in Eq. (57), which is equivalent to

$$R_{sh} = 2GM_{BH}/c^2 \leq a - R - \Delta r. \quad (60)$$

Finally, so that the assumption of a Roche geometry is valid, it should be possible for tidal synchronization of the neutron star to be maintained. Bildstein & Cutler (49) considered this, and derived an upper limit for the separation a_{syn} at which tidal synchronization could occur by integrating the maximum torque on the neutron star as it spirals in from infinity and finding where the neutron star spin frequency could first equal the orbital frequency. They find

$$a_{syn} \leq \frac{M_{BH}^2 m_{ns}^2}{400M^3} \left(\frac{R}{m_{ns}} \right)^6, \quad (61)$$

which translates to

$$400 \left(\frac{GM_{BH}}{Rc^2} \right)^5 \frac{a}{R_\ell} \frac{(1+q)^3}{q} \leq 1. \quad (62)$$

Next we consider the effect of putting some of the angular momentum into an accretion disc. Following the discussion of Ref. (49), we assume an accretion disc contains an amount of angular momentum that grows at the rate

$$\dot{J}_d = -(1-f)M^{3/2}a^{1/2}(1+q)^{-4}\dot{q}, \quad (63)$$

where f is a parameter, taken to be a fit to the numerical results of Hut & Paczyński (50):

$$f = 5q^{1/3}/3 - 3q^{2/3}/2. \quad (64)$$

We then find the new condition for angular momentum conservation to be

$$\dot{J} + \dot{J}_d = \dot{J}_{GW}, \quad (65)$$

which yields

$$\dot{q} \left[\frac{\alpha}{2} - \frac{1}{6} + \frac{f - q^2}{1+q} \right] \geq -\frac{32}{5} \frac{G^3}{c^5} \frac{q^2 M^3}{(1+q)a^4}. \quad (66)$$

Therefore, the new condition for stable mass transfer is

$$(q^2 - f)/(1 + q) \leq \alpha/2 - 1/6. \quad (67)$$

The case $f = 1$ corresponds to neglecting the existence of an accretion disc.

It remains to determine when an accretion disc is likely to form. Initially, matter flowing from the neutron star to the black hole through the inner Lagrangian point passes close to the black hole and falls in. However, as the neutron star spirals away, the accretion stream trajectory moves outside the Schwarzschild radius. When the trajectory doesn't even penetrate the marginally stable orbit, an accretion disc will begin to form. Particle trajectory computations of the Roche geometry by Shore, Livio & van den Huevel (51) suggest that its closest approach to the black hole is

$$R_c = a(1 + q)(0.5 - 0.227 \ln q)^4. \quad (68)$$

Equating R_c to $6GM_{BH}/c^2$ yields

$$(0.5 - 0.227 \ln q)^4(1 + q) \geq 6 \frac{GM_{BH}}{Rc^2} \frac{R_\ell}{a}. \quad (69)$$

These constraints and allowed regions for stable mass transfer are shown in Fig. 12. Apparently, stable mass transfer ceases when $m_{ns} \approx 0.14 M_\odot$ if the formation of an accretion disc is ignored. If the effects of disc formation are included, the stable mass transfer ceases when $m_{ns} \approx 0.22 M_\odot$. In both cases, the neutron star mass remains above its minimum mass (about $0.09 M_\odot$ for the equation of state used here). Thus, the neutron star does not “explode” by reaching its minimum mass.

Fig. 13 shows the time development of the orbital separation a and the neutron star's mass and radius during the inspiral and stable mass transfer phases. Solid lines are calculated assuming there is no accretion disc formed, while dashed lines show the effects of accretion disc formation. The time evolutions during stable mass transfer are obtained from Eq. (57) and Eq. (66), using $\dot{m}_{ns} = \dot{q}M/(1 + q)^2$. With disc formation, the mass transfer is accelerated and the duration of the stable mass transfer phase is shortened considerably. Also, the neutron star spirals out to a smaller radius, and does not lose as much mass, as in the case when the accretion disc is ignored.

Therefore, if stable mass transfer can take place, the timescale over which mass transfer occurs will be much longer than an orbital period, and lasts perhaps a few tenths of a second. This is not long enough to explain gamma-ray bursts. However, we have also seen the likelihood that an accretion disc

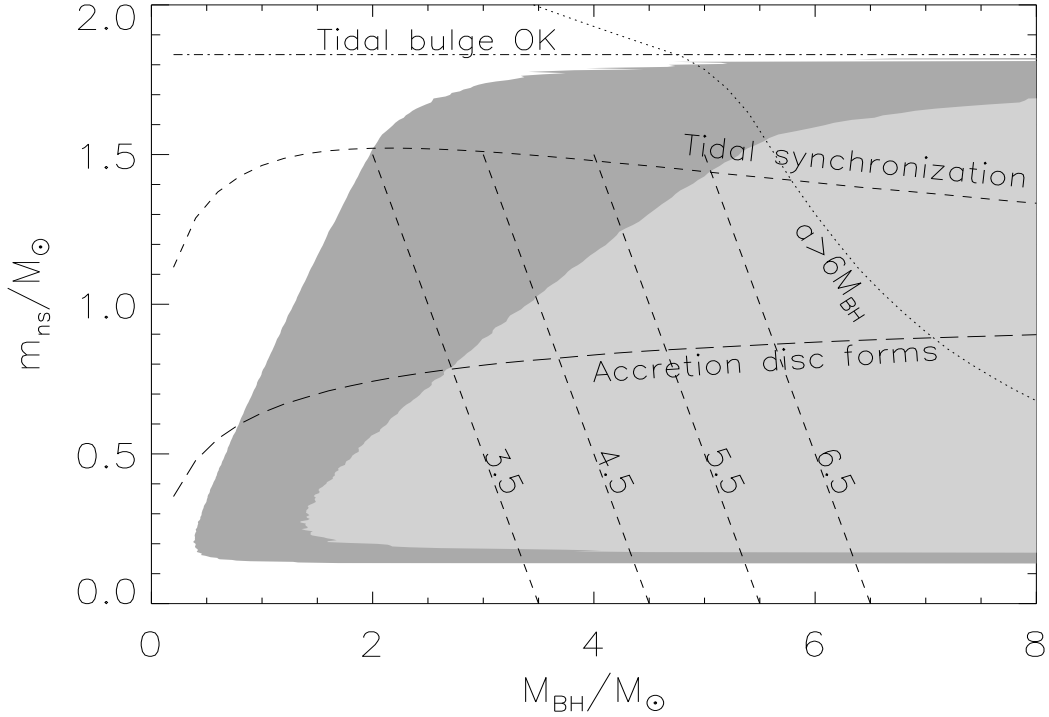


Fig. 12. The dark and light shaded regions show the binary masses for which mass transfer in a black hole–neutron star binary will be stable in the absence of, and the presence of, an accretion disc. The constraints Eq. (58) ($a > 6M_{BH}$), Eq. (60) (Tidal bulge OK), Eq. (62) (Tidal synchronization), and Eq. (69) (Accretion disc forms) are shown by the appropriately labelled curves. The parallel, diagonal, dashed lines show evolutionary tracks for the labelled total BH+NS masses, beginning in each case with $m_{ns} = 1.5 M_{\odot}$.

forms is quite large. Furthermore, the accretion disc extends to about 100 km. Even though this is considerably less than Ref. (45) estimated, the lifetime of such an extended disc is considerable. To order of magnitude, it is given by the viscous dissipation time, or

$$\tau_{visc} \sim \frac{D^2}{\alpha c_s H}. \quad (70)$$

Here D is the radial size of the disc, α is the disc’s viscosity parameter, c_s is the sound speed and H is the disc’s thickness. Note that $c_s \approx \Omega H$ where $\Omega = 2\pi/P = \sqrt{GM_{BH}/D^3}$ is the Kepler frequency. Thus,

$$\tau_{visc} \sim \frac{P}{2\pi\alpha} \left(\frac{D}{H} \right)^2. \quad (71)$$

Since the magnitude of α is still undetermined, and usually quoted (52) to be about 0.01, and H is likely to be of order R , we find $\tau_{visc} \sim 230$ s for our case.

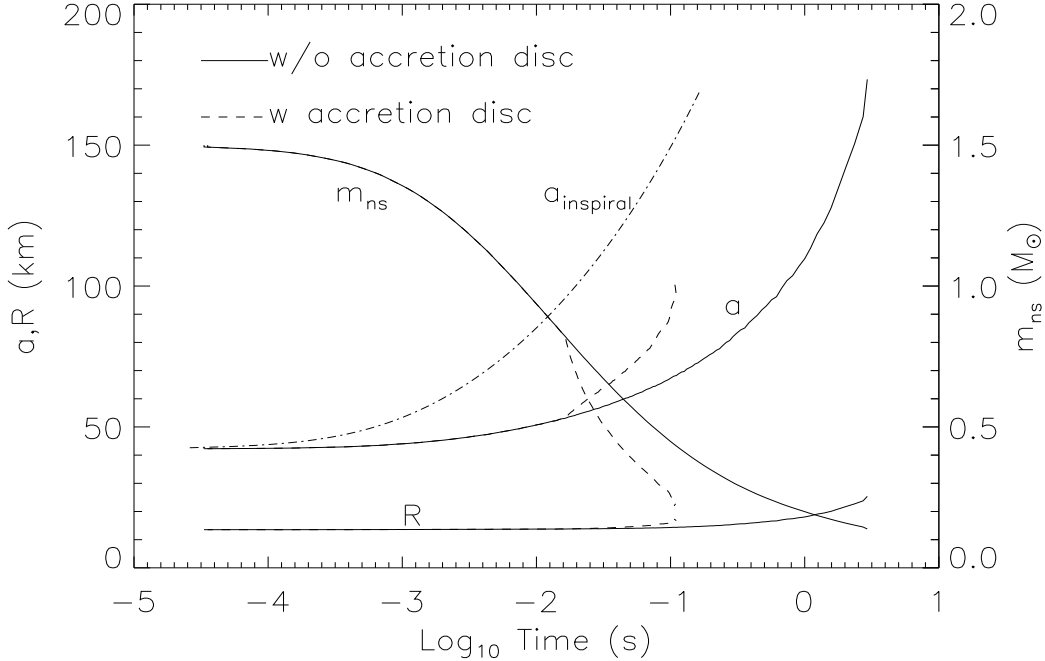


Fig. 13. The separation of a $1.5 M_{\odot}$ neutron star with a $3 M_{\odot}$ black hole during a merger is indicated by the dot-dashed line during inspiral and by a solid line in the outspiral during stable mass transfer. Other curves show the neutron star mass and radius during the stable mass transfer (outspiral) phase. Solid (dashed) lines are computed by ignoring (including) the effects of an accretion disc.

This alleviates the timescale problem for these models. Numerical simulations of such events are in progress, and it remains to be seen if a viable gamma-ray burst model from neutron star–black hole coalescence is possible. If it is, a great deal of the credit should rest with Dave.

We thank Ralph Wijers for discussions concerning accretion disks.

References

- [1] G. Baym, H.A. Bethe, and C.J. Pethick, *Nucl. Phys.* **A175** (1971) 225.
- [2] J.M. Lattimer, C.J. Pethick, D.G. Ravenhall, and D.Q. Lamb, *Nucl. Phys.* **A432** (1985) 646.
- [3] J.M. Lattimer and F.D. Swesty, *Nucl. Phys.* **A535** (1991) 331.
- [4] J.P. Blaizot, J.F. Berger, J. Dechargé, and M. Girod, *Nucl. Phys.* **A591** (1995) 431; D.H. Youngblood, H.L. Clark, and Y.-W. Lui, *Phys. Rev. Lett.* **82** (199) 691.

- [5] J.M. Pearson, *Phys. Lett.* **B271** (1991) 12.
- [6] J.M. Lattimer, in *Nuclear Equation of State*, A. Ansari and L. Satpathy, eds., World Scientific, Singapore, 1996, p. 83.
- [7] E. Lipparini and S. Stringari, *Phys. Lett.* **B112** (1982) 421.
- [8] K. Sato, *Prog. Theor. Phys.* **53** (1975) 595; **54** (1975) 1325.
- [9] J.M. Lattimer, A. Burrows, and A. Yahil, *Astrophys. J.* **288** (1985) 644.
- [10] F.D. Swesty, J.M. Lattimer, and E. Myra, *Astrophys. J.* **425** (1994) 195.
- [11] J.M. Lattimer and M. Prakash, in preparation (2000).
- [12] D.G. Ravenhall and C.J. Pethick, *Astrophys. J.* **424** (1994) 846.
- [13] B. Link, R.I. Epstein, and J.M. Lattimer, *Phys. Rev. Lett.* **83** (1999) 3362.
- [14] L. Titarchuk, *Astrophys. J.* **429** (1994) 340; F. Haberl and L. Titarchuk, *Astron. Astrophys.* **299** (1995) 414.
- [15] J.M. Lattimer, M. Prakash, D. Masak, and A. Yahil, *Astrophys. J.* **355** (1990) 241.
- [16] N.K. Glendenning, *Phys. Rev. D* **46** (1992) 4161.
- [17] D. Page, *Astrophys. J.* **442** (1995) 273.
- [18] F.M. Walter, S.J. Wolk and R. Neuhäuser, *Nature* **379** (1996) 233; F.M. Walter, *et al.*, *Nature* **389** (1997) 358.
- [19] R.W. Romani, *Astrophys. J.* **313** (1987) 718.
- [20] P. An, J.M. Lattimer, M. Prakash and F.M. Walter, in preparation (2000).
- [21] B. Friedman and V.R. Pandharipande, *Nucl. Phys.* **A361** (1981) 502.
- [22] V. R. Pandharipande and R. A. Smith, *Nucl. Phys.* **A237** (1975) 507.
- [23] R.B. Wiringa, V. Fiks, and A. Fabrocine, *Phys. Rev.* **C38** (1988)1010.
- [24] A. Akmal and V.R. Pandharipande, *Phys. Rev.* **C56** (1997) 2261.

- [25] H. Müller and B.D. Serot, *Nucl. Phys.* **606** (1996) 508.
- [26] H. Müther, M. Prakash, and T.L. Ainsworth, *Phys. Lett.* **199** (1987) 469.
- [27] L. Engvik, M. Hjorth-Jensen, E. Osnes, G. Bao, and E. Østgaard, *Phys. Rev. Lett.* **73** (1994) 2650.
- [28] M. Prakash, T.L. Ainsworth, and J.M. Lattimer, *Phys. Rev. Lett.* **61** (1988) 2518.
- [29] N.K. Glendenning and S.A. Moszkowski, *Phys. Rev. Lett.* **67** (1991) 2414.
- [30] N.K. Glendenning and Jürgen Schaffner-Bielich, *Phys. Rev.* **C60** (1999) 025803.
- [31] M. Prakash, J. R. Cooke and J. M. Lattimer, *Phys. Rev.* **52** (1995) 661.
- [32] M. Prakash, I. Bombaci, M. Prakash, J.M. Lattimer, P. Ellis, and R. Knorren, *Phys. Rep.* **280** (1997) 1.
- [33] H.A. Buchdahl, *Astrophys. J.* **147** (1967) 310.
- [34] M. Prakash, in *Nuclear Equation of State*, A. Ansari and L. Satpathy, eds., World Scientific, Singapore, 1996, p. 229.
- [35] M.S.R. Delgaty and K. Lake, *Computer Physics Communications* **115** (1998) 395.
- [36] R.C. Tolman, *Phys. Rev.* **55** (1939) 364.
- [37] M.C. Durgapal and A. K. Pande, *J. Pure & Applied Phys.* **18** (1980) 171.
- [38] J.M. Lattimer and A. Yahil, *Astrophys. J.* **340** (1989) 426.
- [39] J.M. Lattimer and D.N. Schramm, *Astrophys. J. (Letters)*, **192** (1974) L145; *Astrophys. J.* **210** (1976) 549.
- [40] R.A. Hulse and J.H. Taylor, *Astrophys. J. (Letters)*, **195** (1975) L51.
- [41] J.M. Lattimer, Ph.D thesis, University of Texas at Austin, unpublished (1976).
- [42] P.C. Peters, *Phys. Rev.* **136** (1964) 1224.

- [43] D. Eichler, M. Livio, T. Piran, and D.N. Schramm, *Nature* **340** (1989) 126.
- [44] C.S. Kochanek, *Astrophys. J.* **398** (1992) 234.
- [45] S.F. Portegies Zwart, *Astrophys. J. (Letters)*, **503** (1998) L53.
- [46] L. Fishbone, *Astrophys. J. (Letters)*, **175** (1972) L155.
- [47] B. Paczyński, *Ann. Rev. Astron. Astrophys.* **9** (1971) 183.
- [48] P.P. Eggleton, *Astrophys. J.* **368** (1978) 369.
- [49] L. Bildstein and C. Cutler, *Astrophys. J.* **400** (1992) 175.
- [50] P. Hut and B. Paczyński, *Astrophys. J.* **284** (1984) 675.
- [51] S. Shore, M. Livio, and E.P.J. van den Huevel, in *Interacting Binaries*, Saas-Fee Advanced Course 22 for Astronomy and Astrophysics, 1992, 145.
- [52] A. Brandenburg, A. Nordlund, R.F. Stein, and U. Torkelsson, *Astrophys. J. (Letters)* **458** (1996) L45.